Paleoproterozoic U Mineralization in Huayangchuan Deposit, Xiaoqinling Area: Evidence From the U-Rich Granitic Pegmatite

Putao Li , Yongjun Li * , Pingyang Gu , Shiping He , Yujun Zhuang , Ruiming Chen

Posted Date: 13 June 2023

doi: 10.20944/preprints202306.0870.v1

Keywords: Southern Margin of North China Craton; Xiaoqinling; Huayangchuan; Uranium; Pegmatite; Paleoproterozoic; Mineralization age

Article

Paleoproterozoic U mineralization in Huayangchuan Deposit, Xiaoqinling Area: Evidence from the U-Rich Granitic Pegmatite

Putao Li [1,2], Yongjun Li [1,*], Pingyang Gu [2], Shiping He [2], Yujun Zhuang [2] and Ruiming Chen [2]

[1] Chang'an University,School of Earth Science and Resources, Xi'an 710054, China
[2] Xi'an Center of China Geological Survey, Xi'an 710119, Shannxi, China
* Correspondence: yongjunl@chd.edu.cn

Abstract: The Huayangchuan uranium deposit, located in the west of the Xiaoqinling belt on the southern margin of the North China Craton, is a polymetallic deposit dominated by U, Nb, Pb, and rare earth elements. The Huayangchuan uranium deposit, discovered in the 1950s, has long been known as a carbonatite-type uranium deposit. Recently, new geological work has found uranium mineralisation in many granitic pegmatite veins in the Huayangchuan deposit and adjacent areas. Here, we report a systematic investigation of the petrography, whole-rock geochemistry, zircon U-Pb ages, and in situ Lu-Hf isotopic characteristics of newly discovered U-rich granitic pegmatite veins in the west of Huayangchuan deposit. The petrological results showed that the lithology of the samples is equivalent to that of granite. The U-Pb ages of zircon were 1826.3 ± 7.9 and 1829 ± 11 Ma. Microscopically, the symbiotic characteristics of zircon, betafite, and uraninite exist in the intergranular fissures of K-feldspar and quartz, reflecting metallogenic phenomena in the rock formation process. Almost all whole-rock samples were rich in SiO_2 (64.37–70.69 wt.%), total alkalis (K_2O+Na_2O = 8.50–10.30 wt.%), and Al_2O_3 (12.20–14.41 wt.%), but poor in Ti_2O (0.23–0.73 wt.%), MgO (0.38–0.90 wt.%), P_2O_5 (0.14–0.83 wt.%), MnO (0.04–0.57 wt.%). Additionally, they showed enrichment of LILEs (such as Rb, Ba, Th, U, and K), depletion of HFSEs (such as Ta, Nb, P, Ti, and Hf), no alkaline dark minerals, and the characteristics are typical of intraplate A1-type granite. The A1-type granite displayed low zircon $\varepsilon_{Hf}(t)$ values (-19.42– -15.02) with zircon two-stage Hf model aged 3.10–2.76 Ga, indicating that the U-rich granitic pegmatite was derived predominantly from partial melting of the ancient continental crust (such as the early Taihua group formed in Archean-Neoarchean). Combined with the above results and regional geological data, the U-rich granitic pegmatite discovered in the Huayangchuan deposit was related to granite magma activity that formed in a post-collisional regime after the Luliang movement in the late Palaeoproterozoic. This study suggests that future uranium prospecting work in this area should focus on late Palaeoproterozoic U-rich granitic pegmatites.

Keywords: Southern Margin of North China Craton; Xiaoqinling; Huayangchuan; uranium; pegmatite; Paleoproterozoic; mineralization age

1. Introduction

The Huayangchuan U deposit in the Qinling Orogenic Belt (Central China; QLOB) was discovered during the 1950s. In the last decade, the Huayangchuan deposit has been recognised as a giant carbonate-hosted U-polymetallic deposit characterised by dominant U with abundant Nb, rare earth elements (REE), and Pb resources [1–3]. Since its discovery, it has been famous worldwide for the rare presence of carbonatite-related U–Nb–REE mineralisation [4–6]. Many studies have been published on carbonatites in Huayangchuan, including their chronology, petrography, and geochemistry, all of which point to an igneous origin of carbonatites in QLOB in the evolutionary background of the Late Triassic [7–13]. Apart from Huayangchuan, the district also contains other large deposits, such as the Xigou carbonatite-related Mo deposit and Huanglongpu carbonatite-

 doi:10.20944/preprints202306.0870.v1

related Mo–Pb(-Re) deposit. Regionally, these typical deposits are part of the Triassic carbonatite metallogenic belt of North Qinling.

Recently, new geological work has discovered U mineralisation in many granitic pegmatite veins in the Huayangchuan deposit and in adjacent peripheral areas. The U and Nb contents of some of the granitic pegmatite veins reached industrial grade. Field observations and laboratory research have shown that the metallogenic characteristics of U-rich granitic pegmatite veins are different from those of U-rich carbonate veins in the Huayangchuan deposit area. However, studies on the chronology, petrography, and geochemistry of U-rich granitic pegmatite veins are scarce and only a few have been conducted. In this study, we present an investigation of the petrography, whole-rock geochemistry, zircon U–Pb ages, and in situ Lu–Hf isotopic data for the U-rich granitic pegmatite veins in the Huayangchuan deposit. Integrating our new results for U-rich granitic pegmatites, we discuss the industrial minerals, diagenetic and metallogenic epoch, petrogenesis, and tectonic setting. The study of U-rich granitic pegmatites indicates that late Palaeoproterozoic U-mineralisation occurred in the Huayangchuan deposit, which can provide a new target for U-prospecting in this area and should attract our attention.

2. Regional and Deposit Geology

The Qinling Orogenic Belt (QLOB), an important tectonic unit in central China (Figure 1a), has undergone a prolonged and complex tectonic evolution [14]. The Huayangchuan deposit is located in Shaanxi Province, central China, and geologically located in west of the Xiaoqinling tectonic belt on the southern margin of the North China Craton (Figure 1a,b). The Xiaoqinling tectonic belt is a metamorphic core complex (Figure 1c), and its exposure range is limited by a series of deep and large boundary fault zones [15]. Various magmatic rocks and veins of different ages intrude into the metamorphic core complex, making the uranium deposit in this area with complex genesis by "ancient basement, deep fault, and magmatism".

According to the metallogenic characteristics of uranium in the area, the geological bodies closely related to uranium mineralisation mainly include the Taihua group, Huayangchuan fault zone, and Laoniushan and Huashan granites. Local stratigraphic units in the Huayangchuan area comprise the Archean Taihua group, which is a high-grade metamorphosed and the main outcropping sequence. The Taihua group provided magma sources and materials for various diagenetic and metallogenic events. Major faults (e.g., Taiyao, Xiaohe, Huayangchuan, and Luonan–Luanchuan; Figure 1c) are all NE- or EW-trending, superimposed by NS-trending secondary faults and fractures. The NE-trending Huayangchuan Fault controls the major distribution of ore bodies in Huayangchuan. In Huayangchuan, the magmatic rocks mainly comprise Proterozoic granite and pegmatite, Triassic carbonatite dikes, and Jurassic-Cretaceous granitoids (Figure 2).

Numerous U-rich granitic pegmatite veins have been found in the western and peripheral areas of the Huayangchuan deposit. Geological field observations showed that the U-rich granitic pegmatite intruded into the Taihua Group in a large single vein (Figure 3a,b). Its exposed width was over 1–3 m, length reached 100 m, extension direction was nearly E–W, and dip angle was approximately 50°–70°. The chloritisation and weathering of the contact zone formed by pegmatite and the surrounding rock were evident (Figure 3a,b), indicating that the contact zone was a weak area where fluids could easily act. The U and Nb contents in some granitic pegmatite veins reached high industrial grade. Extension of some U-rich granitic pegmatite veins can be observed deep underground through drilling.

 doi:10.20944/preprints202306.0870.v1

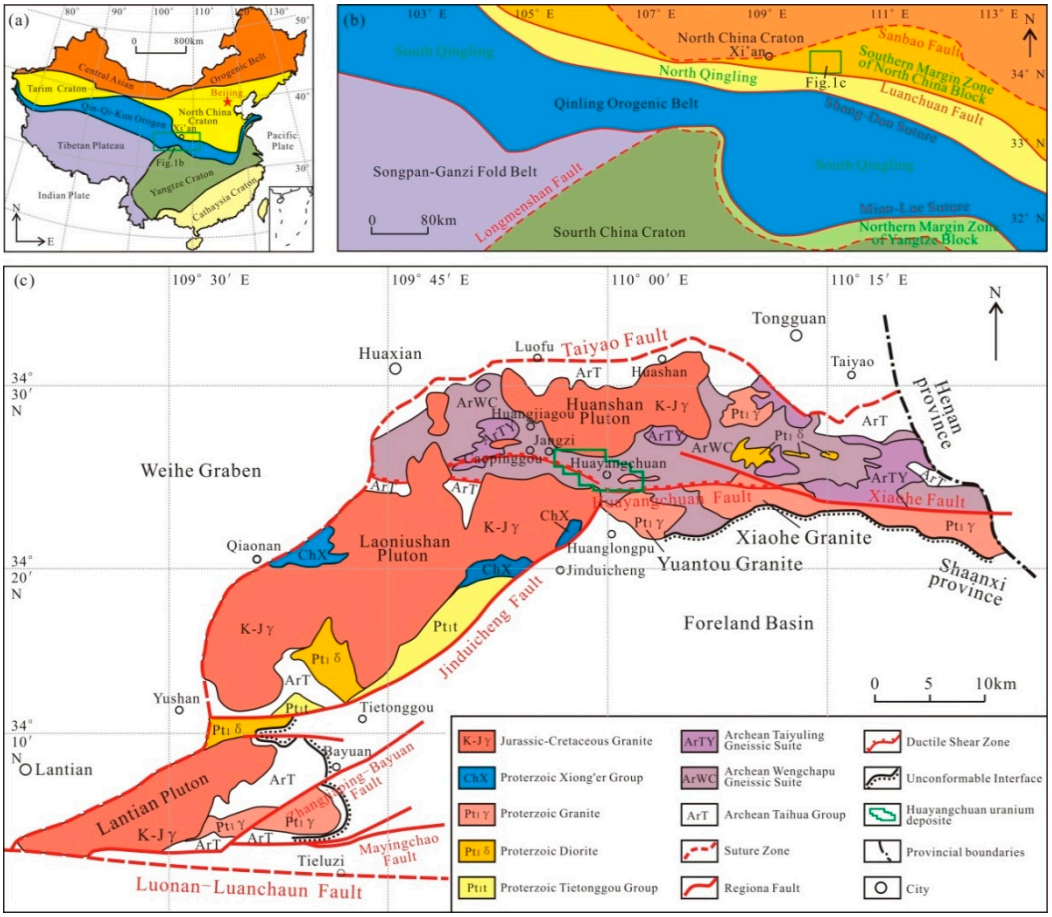

Figure 1. (a) Geologic sketch map of China; (b) Regional tectonic map of Qinling Orogen; (c) Geologic map of the Huayangchuan district (modified from [2]) .

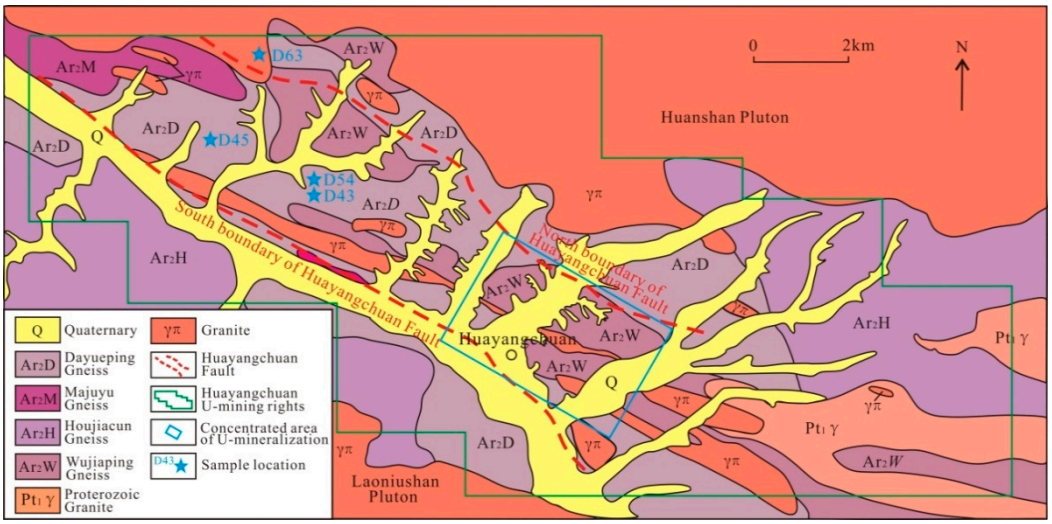

Figure 2. Simplified geologic map of the Huayangchuan deposit (modified from [13]).

 doi:10.20944/preprints202306.0870.v1

Figure 3. Representative images of U-rich granitic pegmatite veins (a)-(b); Ore images of U-rich granitic pegmatite veins (c)- (d).

3. Sample Characteristics

The studied pegmatite samples were collected from the western Huayangchuan deposit (Figure 2). Two representative U-rich granitic pegmatite samples were tested for petrography, whole-rock geochemistry, zircon U–Pb ages, and in situ Lu–Hf isotopes.

3.1. Petrographic Characteristics of Samples

The U-rich granitic pegmatites were mainly composed of quartz (approximately 15–25 wt.%), K-feldspar (approximately 50–60 wt.%), plagioclase (approximately 10–20 wt.%), and small amounts of biotite, hornblende, and accessory minerals. Its total mineral composition was approximately equivalent to that of granite. The contact boundary formed by gneissic xenoliths of the Taihua Group in the U-rich granitic pegmatites was observed under a polarising microscope (Figure 4a). The rock-forming minerals of the U-rich granitic pegmatites exhibited an evidently coarse pegmatitic texture (Figure 4b). In addition, zircon particles with good crystal forms were observed between the inter-crystalline fractures of K-feldspar and quartz (Figure 4c). Meanwhile, intrusion of quartz veinlets into the plagioclase fissure of gneiss was observed (Figure 4d), which suggests that the magmatic hydrothermalism occurred during the formation of U-rich granitic pegmatite.

 doi:10.20944/preprints202306.0870.v1

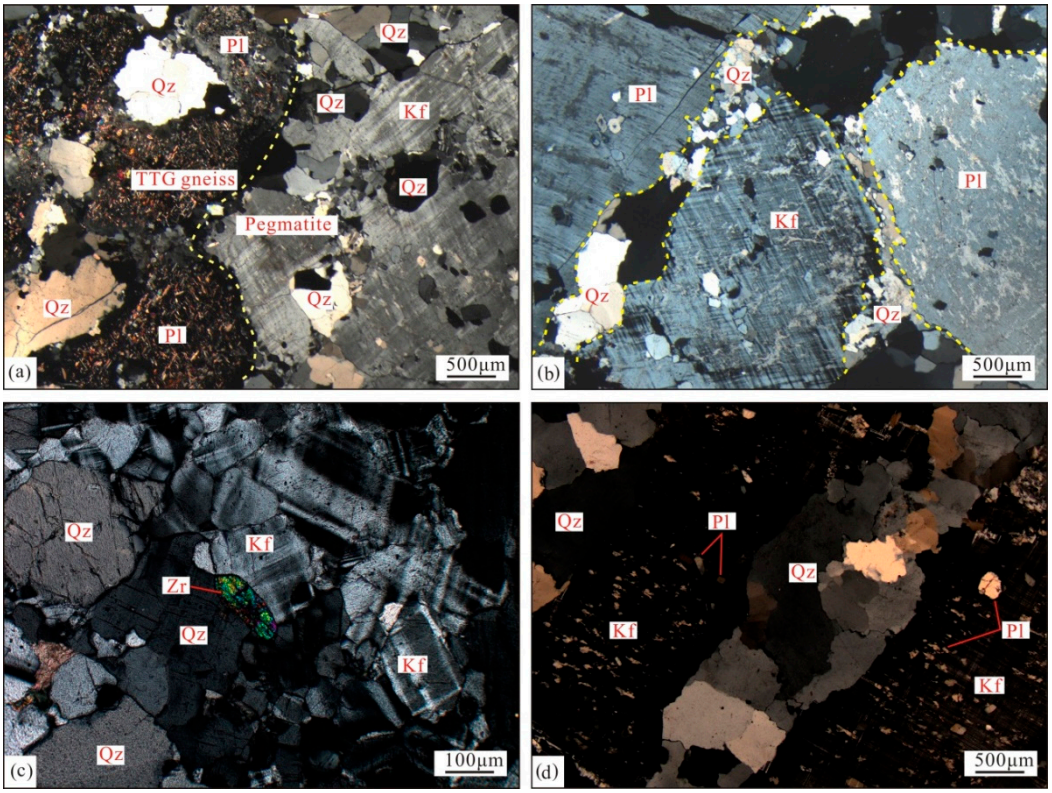

Figure 4. (a) Boundary between pegmatite and gneiss xenolith; (b) Pegmatitic texture; (c) Zircon with intact crystal form; (d) Quartz veinlets in gneiss fractures. Qz: Quartz, Pl: Plagioclase, Kf: K-feldspar, Zr: zircon.

3.2. Characteristics of Uranium and Zircon

Scanning electron microscopy (SEM) showed that the main uranium minerals in the U-rich granitic pegmatite were betafite and a small amount of uraninite. The symbiotic relationship between zircon and uranium minerals provides supporting evidence for the age of diagenesis and mineralisation.

3.2.1. Betafite

Betafite is mainly hosted in the intergranular fissures of rock-forming minerals in the U-rich granitic pegmatite, showing a relatively complete crystal morphology (Figure 5a,b). The aggregation of betafites was also observed in the U-rich granitic pegmatite (Figure 5c,d). In addition, the filling of quartz, K-feldspar, and other minerals can also be observed in the holes in the betafite (Figure 5d). These characteristics reveal that betafites and rock-forming minerals were formed during the diagenetic process at the same stage. Theoretically, betafite is an equiaxed octahedral crystal. However, the crystal shape of betafite in the U-rich granitic pegmatite was incomplete, and the developed fractures often extended into rocks (Figure 5a,b). These characteristics indicate that the U-rich granitic pegmatite may have been affected by tectonic stress in the later stages, which often destroyed the crystal form of the betafite.

 doi:10.20944/preprints202306.0870.v1

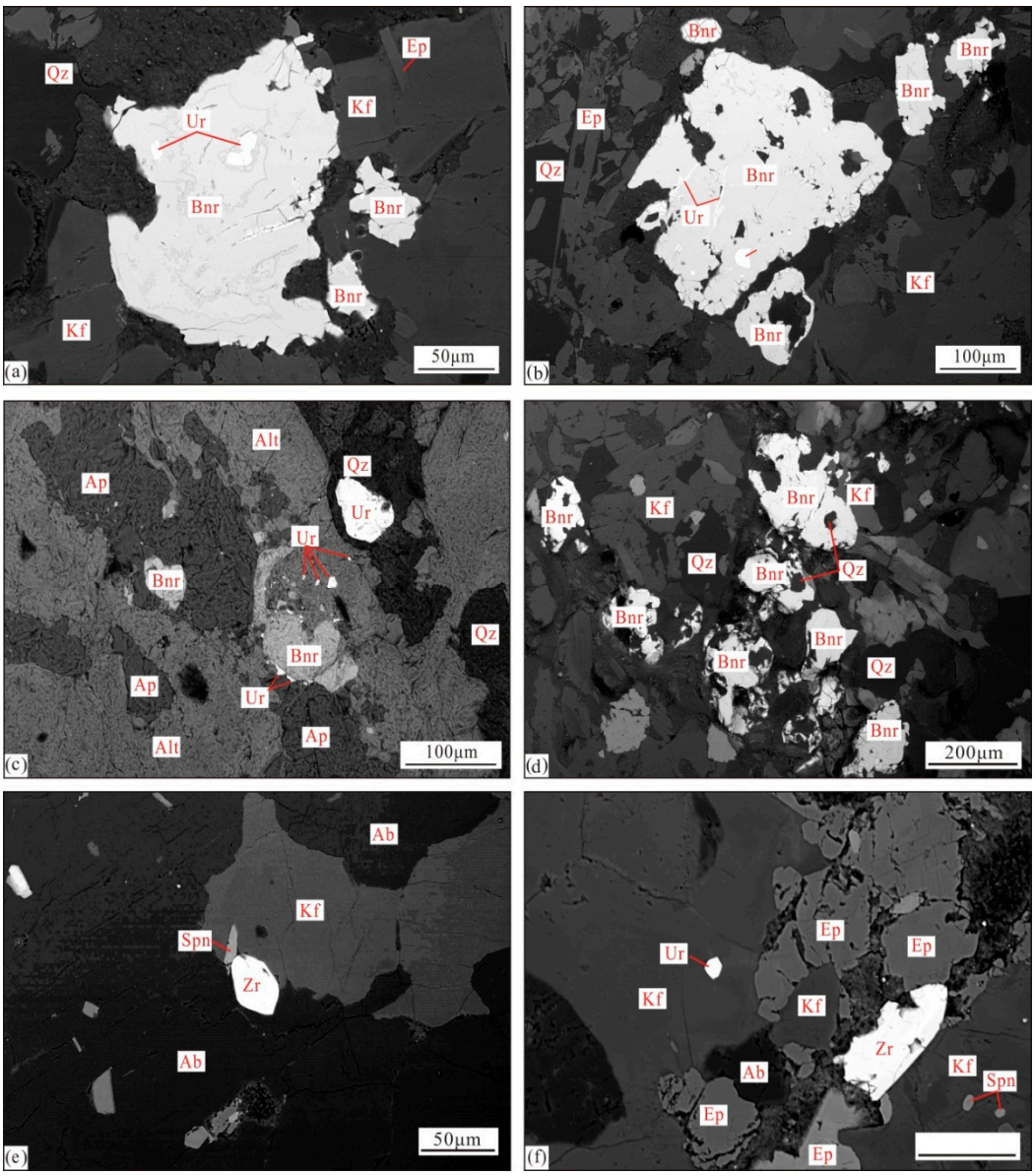

Figure 5. (a) Betafite and its encapsulated uraninite; (b) Betafite and its internal fissure uraninite; (c) Betafite and its edge growing uraninite; (d) Betafite aggregates between K-feldspar and quartz; (e) Zircon between K-feldspar and albite; (f) Zircon from intergranular fissures of K-feldspar. Qz: Quartz, Kf: K-feldspar, Ab: Albite, Bnr: Betafite, U: Uraninite, Alt: Allanite, Ep: Epidote, Spn: Sphene, Zr: Zircon.

3.2.2. Uraninite

Uraninite in U-rich granitic pegmatite is characterised by low content and fine grain size and is associated with betafite, which indicates that it is closely related to the material source and genesis. Under a scanning electron microscope, some uraninite was seen wrapped in betafite (Figure 5a), and some uraninite existed on the outer edge (Figure 5b) or internal fissure of the betafite (Figure 5c). Because the crystallisation temperature of uraninite is higher than that of betafite, the formation of uraninite wrapped in betafite may have occurred earlier than that of betafite. During the diagenesis of U-rich granitic pegmatites, uranium minerals gradually change from uraninite to betafite with a decrease in temperature. The uraninite grains that grew in the internal fissures of betafite or on the outer edge of betafite were probably formed by the recrystallisation of U from betafite.

 doi:10.20944/preprints202306.0870.v1

3.2.3. Zircon

The genetic type of zircons and the symbiotic relationship between zircons and ore minerals are important bases for determining the age of diagenesis and mineralisation. Zircons with a columnar shape and intact crystal form can be observed under a scanning electron microscope (Figure 5e,f), which showed the same characteristics as zircon in the cathodoluminescence (CL) images. All these show the characteristics of magmatic zircons. Zircons occurred in the intergranular fissures of K-feldspar and were associated with uraninite (Figure 5f). The above occurrence characteristics of zircons indicate mineralisation of the U-rich granitic pegmatite during diagenesis. Therefore, the zircon age can provide supporting chronological evidence for diagenesis and mineralisation.

4. Analytical Methods

4.1. Zircon U–Pb Geochronology

Zircon crystals were separated using heavy-liquid and magnetic methods. Separated zircons were carefully handpicked under a binocular microscope. The selected high-quality zircons were further mounted in epoxy resins and finally polished to approximately half their thickness for analysis. CL images were captured at the Xi'an Center of Geological Survey, CGS (China) to investigate internal structures of analysed zircons and to select target positions for U–Pb dating and Hf isotopic analysis. Zircon U–Pb dating with a beam size of 30 μm was conducted using LA–ICP–MS at the Key Laboratory for the study of focused Magmatism and Giant ore Deposits, MLR, Xi'an Center of Geological Survey, CGS (China), using a system of a Geolas 200 M equipped with a 193 nm ArFexcimer laser. Zircon 91500, GJ-1, and NIST610 were used as reference materials for U–Pb dating and instrument optimisation. The U–Th–Pb ratios were calculated using Glitter 4.4. Concordia diagrams and weighted mean calculations were performed using the Isoplot/Ex.3 software [16]. Common Pb compositions were calibrated using the method described by Andersen [17].

4.2. Major and Trace Element Analyses

Twenty fresh whole-rock samples were collected for major and trace element analyses. Major- and trace-element analyses were performed at the Key Laboratory for the Study of Focused Magmatism and Giant Ore Deposits in Xi'an, (China). Whole-rock geochemical analyses were performed using X-ray fluorescence (XRF) and ICP-MS, with analytical errors <3 wt.% for most elements. Loss on ignition (LOI) was estimated using an electronic analytical balance at constant temperature of approximately 1000 °C. The detailed procedures followed are as described by Yang et al. [18].

4.3. Zircon Hf Isotopic Analyses

Zircon Lu–Hf isotope measurements were performed using a Geolas-Pro laser ablation system coupled to a Neptune multiple-collector inductively coupled plasma mass spectrometry (ICP–MS). Details of the instrumental conditions and acquisition were similar to those described in previous studies [19]. A stationary laser ablation spot with a beam diameter of 32 μm was used for the analyses. During the analysis, zircon GJ-1 was used as the reference standard, yielding a weighted mean $^{176}Hf/^{177}Hf$ ratio of 0.281990–0.282070. The present-day chondritic ratios of $^{176}Hf/^{177}Hf$ and $^{176}Lu/^{177}Hf$ are 0.282772 and 0.0332 [20], respectively. The decay constant for ^{176}Lu is $1.865 \times 10^{-11} a^{-1}$ [21]; these values were used to calculate the ε_{Hf} values. In addition, the depleted mantle single-stage (T_{DM1}) and two-stage model ages (T_{DM2}) were calculated with reference to present-day $^{176}Hf/^{177}Hf$ ratios of 0.28325 and $^{176}Lu/^{177}Hf$ ratios of 0.0384 obtained from the depleted mantle [22].

 doi:10.20944/preprints202306.0870.v1

5. Analytical Results

5.1. Zircon U–Pb Age

Older zircons (>1000 Ma) usually exhibit Pb loss. Under the same initial conditions and geological environment, ^{206}Pb and ^{207}Pb isotopes have synchronous variation characteristics and can maintain a relatively stable ratio [23]. Therefore, the $^{206}Pb/^{238}U$ age was used for zircons younger than 1000 Ma and the $^{206}Pb/^{207}Pb$ age was used for zircons older than 1000 Ma to represent the formation age of zircons. Two representative U-rich granitic pegmatite samples from the western Huayangchuan deposit were dated to determine their diagenetic and metallogenic ages. Most zircons from the samples were translucent–transparent crystals. They had a size range of 150–300 μm long and 100–200 μm wide, with length:width ratios of 2:1–3:1. The CL images of the zircon grains (Figure 6a) displayed clear concentric oscillatory zoning coupled with high Th:U ratios (most were 0.11–0.89, average = 0.56) (Table 1, Table 2), suggesting a magmatic origin [24]. Meanwhile, the chondrite-normalised REE patterns of the zircons were similar to those of typical magmatic zircons (Figure 7a,c), with elevated HREE/LREE ratios (Figure 7b,d), significant positive Ce anomalies, and positive correlations between Th and U [25]. The results of LA–ICP–MS zircon analyses are listed in Table 1, Table 2, as shown in Figure 8a–d. Analyses of forty-three grains from two groups of zircon samples formed a concordant population with a weighted mean $^{206}Pb/^{207}Pb$ age of 1829 ± 11 Ma (MSWD = 1.5, n = 21; Figure 8b) and 1826.3 ± 7.9 Ma (MSWD = 0.97, n = 22; Figure 8d) , respectively. This age was interpreted as the diagenetic age of the U-rich granitic pegmatite.

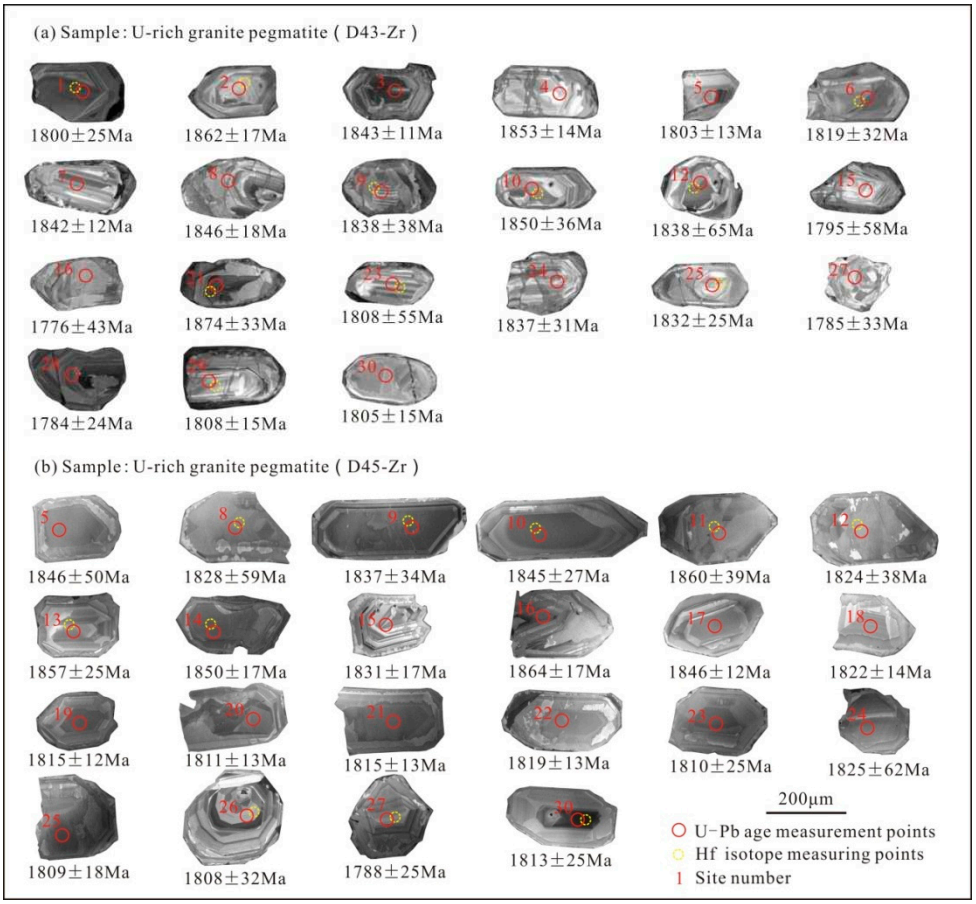

Figure 6. Cathodoluminescence images of zircons from U-rich granitic pegmatite.

 doi:10.20944/preprints202306.0870.v1

Table 1. LA–ICP–MS dating results of zircons from the U-rich granitic pegmatite (D43-Zr).

Site number	Isotopic contents(×10⁻⁶)			Th/U	Isotopic ratios						Ages (Ma)					
	^{232}Th	^{238}U	^{206}Pb		^{207}Pb/^{206}Pb	1σ	^{207}Pb/^{235}U	1σ	^{206}Pb/^{238}U	1σ	^{207}Pb/^{206}Pb	1σ	^{207}Pb/^{235}U	1σ	^{206}Pb/^{238}U	1σ
D43-Zr 1	98.43	259.74	337.46	0.38	0.11004	0.00265	5.13454	0.12013	0.33794	0.00424	1800	25	1842	20	1877	20
D43-Zr 2	167.28	265.39	365.40	0.63	0.11386	0.00211	5.22471	0.09341	0.33234	0.0037	1862	17	1857	15	1850	18
D43-Zr 3	1089.61	843.28	1167.14	1.29	0.11265	0.00151	5.1857	0.06662	0.33343	0.00334	1843	11	1850	11	1855	16
D43-Zr 4	447.03	509.84	711.98	0.88	0.11331	0.00179	5.23058	0.07961	0.33435	0.00351	1853	14	1858	13	1859	17
D43-Zr 5	345.90	780.87	1084.87	0.44	0.11019	0.00167	5.14842	0.07508	0.33843	0.0035	1803	13	1844	12	1879	17
D43-Zr 6	100.15	140.18	197.50	0.71	0.11122	0.0033	5.18751	0.14954	0.33786	0.00476	1819	32	1851	25	1876	23
D43-Zr 7	515.44	577.08	813.96	0.89	0.11263	0.00166	5.24234	0.07419	0.33718	0.00346	1842	12	1860	12	1873	17
D43-Zr 8	205.12	390.15	545.44	0.53	0.11288	0.00221	5.21629	0.09842	0.33479	0.00381	1846	18	1855	16	1862	18
D43-Zr 9	100.38	189.16	266.94	0.53	0.11239	0.00386	5.21178	0.174	0.33595	0.00519	1838	38	1855	28	1867	25
D43-Zr 10	199.06	320.95	457.25	0.62	0.11313	0.00369	5.28373	0.1672	0.33838	0.00508	1850	36	1866	27	1879	24
D43-Zr 11	286.62	347.43	498.58	0.82	0.10964	0.00436	5.26711	0.20378	0.34807	0.00598	1793	45	1864	33	1925	29
D43-Zr 12	53.58	126.46	179.43	0.42	0.11239	0.00614	5.21294	0.27797	0.33607	0.00723	1838	65	1855	45	1868	35
D43-Zr 13	119.28	266.05	372.73	0.45	0.10876	0.00362	5.21221	0.16861	0.34727	0.00518	1779	37	1855	28	1922	25
D43-Zr 14	1283.81	2329.27	3302.17	0.55	0.10729	0.0014	5.04289	0.06241	0.34059	0.00334	1754	10	1827	10	1890	16
D43-Zr 15	142.68	189.51	269.85	0.75	0.10974	0.00536	5.10878	0.24319	0.33736	0.00672	1795	58	1838	40	1874	32
D43-Zr 16	53.86	207.76	294.53	0.26	0.10862	0.00412	5.07892	0.18737	0.33885	0.00557	1776	43	1833	31	1881	27
D43-Zr 17	190.37	443.75	594.51	0.43	0.10451	0.00372	4.36696	0.15106	0.30281	0.00462	1706	41	1706	29	1705	23
D43-Zr 18	115.23	433.07	619.64	0.27	0.10778	0.00275	5.18861	0.12828	0.34889	0.00444	1762	27	1851	21	1929	21
D43-Zr 19	136.61	248.62	364.45	0.55	0.10921	0.00315	5.27281	0.14784	0.34991	0.0048	1786	31	1864	24	1934	23
D43-Zr 20	41.31	157.21	215.51	0.26	0.10369	0.00713	4.30494	0.28889	0.30088	0.0074	1691	87	1694	55	1696	37
D43-Zr 21	125.59	233.32	326.21	0.54	0.11463	0.00352	5.21009	0.15489	0.3294	0.00479	1874	33	1854	25	1835	23
D43-Zr 22	77.29	231.59	318.26	0.33	0.10444	0.00449	4.19583	0.17523	0.29115	0.00509	1704	51	1673	34	1647	25
D43-Zr 23	13.50	209.90	294.81	0.06	0.11053	0.00523	5.15281	0.23697	0.33787	0.00674	1808	55	1845	39	1876	32
D43-Zr 24	144.01	298.90	430.19	0.48	0.1123	0.00323	5.20516	0.14507	0.33594	0.00466	1837	31	1853	24	1867	22
D43-Zr 25	142.41	282.60	403.90	0.50	0.11201	0.00275	5.21895	0.12386	0.3377	0.00426	1832	25	1856	20	1876	21
D43-Zr 26	118.14	273.18	388.65	0.43	0.10738	0.00336	5.1433	0.15635	0.34715	0.00505	1755	34	1843	26	1921	24
D43-Zr 27	92.52	143.41	210.65	0.65	0.10916	0.00331	5.13968	0.15094	0.34125	0.00485	1785	33	1843	25	1893	23
D43-Zr 28	184.27	300.53	438.35	0.61	0.10907	0.00258	5.15027	0.11775	0.34222	0.00421	1784	24	1844	19	1897	20
D43-Zr 29	275.79	443.79	645.12	0.62	0.11055	0.00186	5.17060	0.08305	0.33899	0.00356	1808	15	1848	14	1882	17
D43-Zr 30	224.04	291.71	424.84	0.77	0.11036	0.00184	5.19606	0.08258	0.34124	0.00357	1805	15	1852	14	1893	17

Table 2. LA–ICP–MS dating results of zircons from the U-rich granitic pegmatite (D45-Zr).

Site number	Isotopic contents(× 10⁻⁶)			Th/U	Isotopic ratios						Ages (Ma)					
	^{232}Th	^{238}U	^{206}Pb		^{207}Pb/^{206}Pb	1σ	^{207}Pb/^{235}U	1σ	^{206}Pb/^{238}U	1σ	^{207}Pb/^{206}Pb	1σ	^{207}Pb/^{235}U	1σ	^{206}Pb/^{238}U	1σ
D45-Zr 1	228.10	365.61	485.22	0.62	0.11534	0.00222	5.18495	0.09539	0.32637	0.00352	1885	18	1850	16	1821	17
D45-Zr 2	128.28	309.54	441.36	0.41	0.11556	0.00250	5.15581	0.10680	0.32387	0.00369	1889	21	1845	18	1809	18
D45-Zr 3	80.33	235.43	396.67	0.34	0.11476	0.00283	5.13976	0.12210	0.32510	0.00397	1876	26	1843	20	1815	19
D45-Zr 4	237.05	458.37	608.01	0.52	0.11492	0.00233	5.12766	0.09936	0.32386	0.00358	1879	20	1841	16	1809	17
D45-Zr 5	139.49	331.45	484.36	0.42	0.11286	0.00484	5.18060	0.21601	0.33314	0.00580	1846	50	1849	35	1854	28
D45-Zr 6	189.41	386.22	554.32	0.49	0.10886	0.00461	4.99192	0.20586	0.33278	0.00569	1780	50	1818	35	1852	28
D45-Zr 7	94.63	268.34	358.87	0.35	0.10978	0.00564	5.03454	0.25229	0.33272	0.00662	1796	62	1825	42	1852	32
D45-Zr 8	100.94	330.15	315.84	0.31	0.11174	0.00551	5.04625	0.24235	0.32761	0.00636	1828	59	1827	41	1827	31
D45-Zr 9	250.90	624.89	866.61	0.40	0.11229	0.00348	5.05149	0.15160	0.32634	0.00458	1837	34	1828	25	1821	22
D45-Zr 10	235.17	389.51	457.12	0.60	0.11280	0.00290	5.06802	0.12589	0.32590	0.00409	1845	27	1831	21	1818	20
D45-Zr 11	38.51	145.62	192.54	0.26	0.11372	0.00394	5.08833	0.17119	0.32456	0.00490	1860	39	1834	29	1812	24
D45-Zr 12	55.93	177.01	254.71	0.32	0.11150	0.00375	5.07163	0.16582	0.32992	0.00486	1824	38	1831	28	1838	24
D45-Zr 13	72.56	161.74	263.65	0.45	0.11352	0.00273	5.09377	0.11822	0.32543	0.00396	1857	25	1835	20	1816	19
D45-Zr 14	173.63	401.95	521.82	0.43	0.11311	0.00204	5.03004	0.08685	0.32252	0.00344	1850	17	1824	15	1802	17
D45-Zr 15	180.93	390.31	511.79	0.46	0.11196	0.00202	5.02322	0.08669	0.32538	0.00347	1831	17	1823	15	1816	17
D45-Zr 16	139.81	299.29	395.54	0.47	0.11398	0.00206	5.06457	0.08754	0.32223	0.00344	1864	17	1830	15	1801	17
D45-Zr 17	363.32	496.56	686.98	0.73	0.11286	0.00167	5.04589	0.07128	0.32423	0.00324	1846	12	1827	12	1810	16
D45-Zr 18	307.15	462.25	645.57	0.66	0.11135	0.00174	5.01952	0.07507	0.32691	0.00332	1822	14	1823	13	1823	16
D45-Zr 19	391.09	564.46	708.34	0.69	0.11097	0.00161	4.97956	0.06916	0.32542	0.00324	1815	12	1816	12	1816	16
D45-Zr 20	179.55	495.74	694.59	0.36	0.11071	0.00170	5.02653	0.07396	0.32925	0.00334	1811	13	1824	12	1835	16
D45-Zr 21	257.02	397.13	577.63	0.65	0.11092	0.00171	5.00038	0.07406	0.32693	0.00333	1815	13	1819	13	1823	16
D45-Zr 22	323.16	487.96	678.09	0.66	0.11120	0.00166	5.02863	0.07181	0.32793	0.00331	1819	13	1824	12	1828	16
D45-Zr 23	200.79	325.30	465.12	0.62	0.11064	0.00269	4.95459	0.11685	0.32474	0.00401	1810	25	1812	20	1813	20
D45-Zr 24	141.25	362.66	495.12	0.39	0.11155	0.00586	5.02813	0.25715	0.32690	0.00693	1825	62	1824	43	1823	34
D45-Zr 25	38.10	358.15	559.24	0.11	0.11060	0.00213	5.04176	0.09387	0.33061	0.00367	1809	18	1826	16	1841	18
D45-Zr 26	106.97	234.35	308.37	0.46	0.11053	0.00321	5.10190	0.14402	0.33478	0.00458	1808	32	1836	24	1862	22
D45-Zr 27	79.38	271.86	341.08	0.29	0.10930	0.00263	5.02578	0.11715	0.33349	0.00410	1788	25	1824	20	1855	20
D45-Zr 28	415.24	1008.82	1003.89	0.41	0.11021	0.00187	5.19751	0.08529	0.34206	0.00363	1803	15	1852	14	1897	17
D45-Zr 29	155.56	326.47	508.54	0.48	0.10724	0.00305	5.08513	0.14076	0.34397	0.00461	1753	31	1834	23	1906	22
D45-Zr 30	241.24	915.28	1372.88	0.26	0.11082	0.00265	5.05000	0.11732	0.33056	0.00408	1813	25	1828	20	1841	20

 doi:10.20944/preprints202306.0870.v1

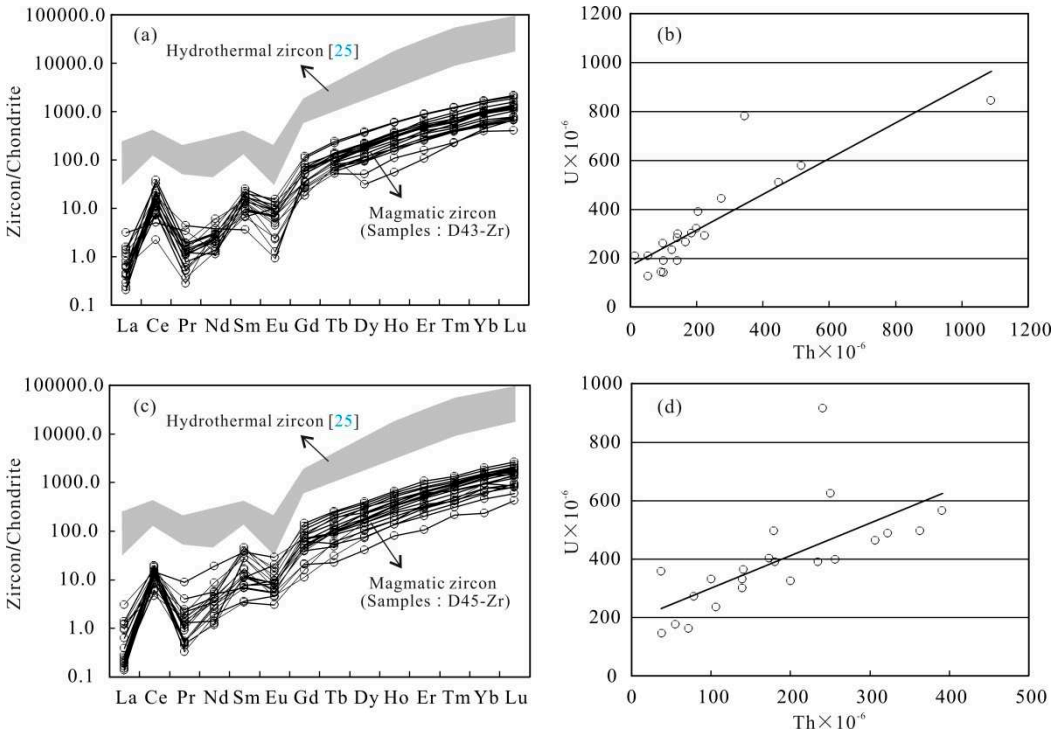

Figure 7. (a) Chondrite-normalised trace multi-element patterns of zircons sample D43-Zr; (b) Th–U element correlation diagram of zircons sample D43-Zr; (c) Chondrite-normalised trace multi-element patterns of zircons sample D45-Zr; (d) Th–U element correlation diagram of zircons sample D45-Zr (Chondrite values are from [26]).

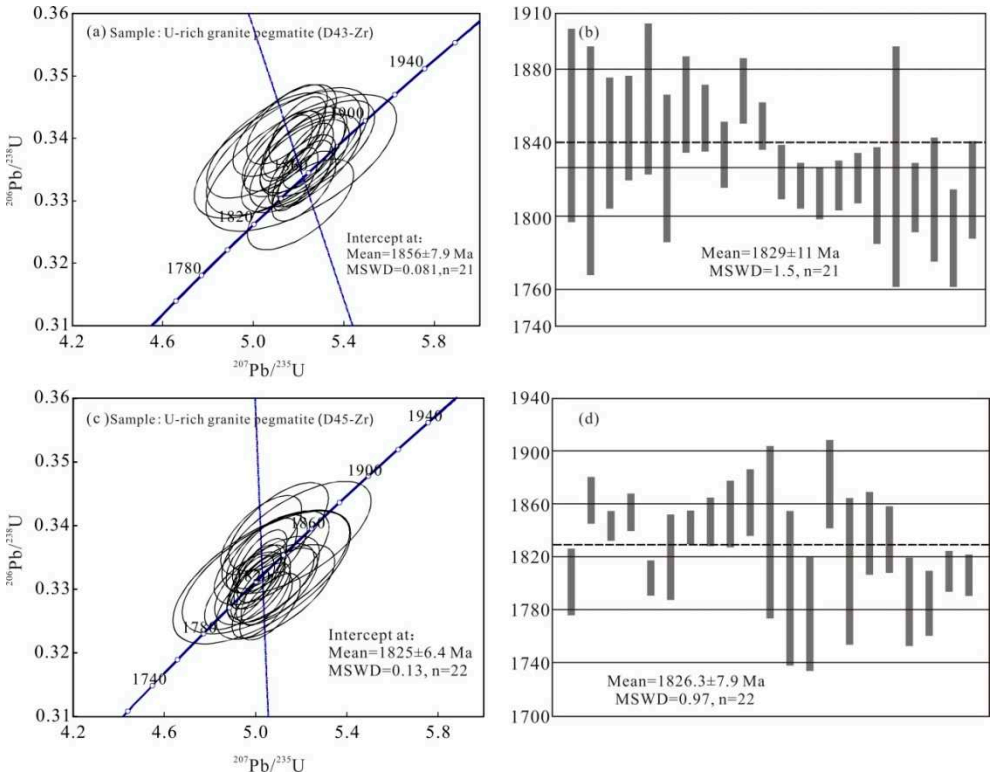

Figure 8. (a) Zircon U–Pb concordia diagrams of sample D43-Zr; (b) Weighted average of zircon U–Pb ages of sample D43-Zr; (c) Zircon U–Pb concordia diagrams of sample D45-Zr; (d) Weighted average of zircon U–Pb ages of sample D45-Zr.

 doi:10.20944/preprints202306.0870.v1

5.2. Major Element Compositions

The major and trace element test data are presented in Table 3 and Table 4 . Most of the U-rich granitic pegmatite samples from the Huayangchuan deposit had low LOI values, indicating that these samples were relatively fresh. The samples were characterised by high concentrations of SiO_2 (64.37–70.69 wt. %) and total alkalis ($Na_2O + K_2O$ = 8.50–10.30 wt.%), higher Al_2O_3 (12.20–14.41 wt.%), but relatively lower concentrations of Ti_2O (0.23–0.73 wt.%), MgO (0.38–0.90 wt.%), P_2O_5 (0.14–0.83 wt.%), and MnO (0.04–0.57 wt.%). Meanwhile, they had low Rittmann index (σ=2.6–4.9, average = 3.8) values. In the SiO_2 vs. $Na_2O + K_2O$ diagram (Figure 9a), SiO_2 vs. K_2O diagram (Figure 9b) and SiO_2 vs. $Na_2O + K_2O$-CaO diagram (Figure 9c), most samples were placed in the alkaline granite field, shoshonitic series and A-Type granite, and generally exhibited metaluminous characteristics (A/CNK = 0.8–0.9, Figure 9d), respectively. In addition, it can also be seen that the U-rich granite pegmatite samples have different major element characteristics with the Paleoproterozoic Yuantou granite [27], Huashan granite and TTG gneiss of Taihua group (Figure 9a–d).

Table 3. Measured contents of major (wt. %), rare earth, and trace elements (ppm) of the U-rich granitic pegmatite.

Sample	D43-YH1	D43-YH2	D43-YH3	D43-YH4	D43-YH5	D45-YH1	D45-YH2	D45-YH3	D45-YH4	D45-YH5
SiO_2	69.92	67.82	70.69	64.37	65.68	66.73	67.05	66.24	66.49	66.13
Al_2O_3	12.50	13.06	12.50	14.41	14.19	14.41	14.38	14.33	14.35	14.37
Fe_2O_3	2.20	3.35	2.55	4.10	3.65	3.46	3.29	3.52	3.72	3.74
FeO	0.88	1.15	0.95	1.40	1.23	1.54	1.33	1.41	1.49	1.50
CaO	2.04	2.22	1.82	1.72	1.84	1.37	1.37	1.23	1.53	1.46
MgO	0.84	0.52	0.38	0.86	0.84	0.88	0.82	0.89	0.86	0.90
K_2O	5.95	5.91	5.57	6.98	6.22	5.22	5.76	5.65	5.02	5.40
Na_2O	3.07	3.17	2.93	3.23	4.08	4.35	3.96	4.11	4.27	4.06
TiO_2	0.26	0.50	0.23	0.65	0.70	0.70	0.66	0.71	0.72	0.73
P_2O_5	0.83	0.17	0.14	0.22	0.22	0.20	0.19	0.22	0.21	0.22
MnO	0.57	0.07	0.04	0.06	0.05	0.07	0.07	0.08	0.06	0.07
LOI	1.43	1.49	1.32	1.55	0.82	0.62	0.63	1.00	0.79	0.82
Tatal	100.49	99.43	99.12	99.55	99.52	99.55	99.51	99.39	99.51	99.40
K_2O+Na_2O	9.02	9.08	8.50	10.21	10.30	9.57	9.72	9.76	9.29	9.46
A/CNK	0.8	0.8	0.9	0.9	0.8	0.9	0.9	0.9	0.9	0.9
A/NK	1.1	1.1	1.2	1.1	1.1	1.1	1.1	1.1	1.2	1.1
σ	3.0	3.3	2.6	4.9	4.7	3.9	3.9	4.1	3.7	3.9
R_1	2089	1881	2269	1350	1328	1532	1577	1486	1585	1546
R_2	383	391	336	368	378	332	328	316	347	342
Rb	64.1	85.9	117	148	118	114	172	187	134	175
Ba	3180	2910	5100	1950	2160	2290	2360	2780	2250	2750
Th	260.00	45.10	79.00	77.50	68.40	60.70	87.60	98.50	76.00	102.00
U	234.00	321.00	289.33	200.50	181.00	89.00	173.00	237.50	109.50	211.50
Ta	0.30	2.18	0.71	1.58	2.10	2.14	2.50	2.86	2.62	2.84
Nb	317.0	104.0	116.0	167.0	156.3	131.3	158.0	201.3	151.0	176.0
Pb	4000	1220	1650	799	870	454	445	835	664	798
Sr	109	146	87.4	118	62.3	132	98.4	138	198	183
Zr	125	34	30.6	33.9	34.3	29.9	38.4	47.6	39.4	48
Hf	22.6	23.0	26.4	25.0	23.9	21.6	26.3	28.5	24.2	27.8
Y	282	100	156	203	243	204	284	336	246	320
Ga	63.50	22.00	28.40	37.10	45.80	39.30	53.50	62.90	47.00	60.40
La	245	76.3	95.4	117	148	125	165	204	153	192
Ce	43.70	13.20	13.80	16.40	19.70	16.40	21.90	26.10	19.10	25.70
Pr	15.00	2.76	2.61	2.76	3.13	2.62	3.41	4.39	3.38	4.23
Nd	33.70	9.86	9.77	11.80	13.60	11.40	14.90	18.60	13.60	17.60
Sm	4.94	1.46	1.30	1.64	1.65	1.37	1.88	2.49	1.90	2.46
Eu	25.10	7.46	6.52	8.14	7.66	6.79	8.77	11.00	8.44	11.60
Gd	4.77	1.48	1.25	1.47	1.40	1.25	1.53	1.90	1.58	2.15
Tb	13.60	4.02	3.44	3.66	3.71	3.26	3.96	5.00	4.21	5.69
Dy	2.05	0.59	0.52	0.55	0.52	0.46	0.57	0.75	0.63	0.76
Ho	13.30	3.80	3.22	3.13	3.19	2.69	3.52	4.39	3.79	4.46
Er	2.03	0.57	0.50	0.48	0.46	0.38	0.54	0.66	0.58	0.63
Tm	1269.69	430.50	613.73	770.13	946.82	745.92	1065.48	1286.18	878.21	1216.68
Yb	5.10	5.76	9.05	9.94	11.86	11.31	12.14	11.51	10.35	10.78

 doi:10.20944/preprints202306.0870.v1

Lu	14.36	17.83	32.82	43.93	51.60	51.37	54.66	51.85	43.97	48.60
REE	4.06	4.77	7.11	7.79	7.76	7.82	8.16	8.10	8.10	7.83
$LREE_N/HREE_N$	2.05	2.10	2.46	3.06	3.46	3.44	3.43	3.44	2.91	3.20
$(La/Yb)_N$	1.19	0.73	0.68	0.60	0.58	0.58	0.57	0.61	0.64	0.60
$(La/Sm)_N$	0.90	0.92	0.98	0.94	0.97	0.84	0.92	0.94	0.79	0.92
$(Gd/Yb)_N$	3.42	3.33	3.99	3.28	3.18	2.83	3.45	3.76	3.19	3.65
δEu	69.92	67.82	70.69	64.37	65.68	66.73	67.05	66.24	66.49	66.13
δCe	12.50	13.06	12.50	14.41	14.19	14.41	14.38	14.33	14.35	14.37
10000×Ga/Al	2.20	3.35	2.55	4.10	3.65	3.46	3.29	3.52	3.72	3.74

NOTE: Abbreviations- LREE: light rare earth element; HREE: heavy rareearth element; REE: rare-earth element; LOI: loss on ignition; $\sigma = (K_2O+Na_2O)^2/(SiO_2-43)$; $Mg^{\#} = Mg^{2+}/(Mg^{2+} + Fe^{2+})$ molar ratio; $R_1 = 4Si^{4+}-11 \times (Na^+ + K^+) - 2 \times (Fe^{3+} + Fe^{2+} + Ti^{4+})$ molar ratio; $R_2 = 6Ca^{2+} + 2Mg^{2+} + Al^{3+}$, molar ratio; $A/CNK = 2Al^{3+}/(Ca^{2+} + 2Na^+ + 2K^+)$ molar ratio; $A/NK = Al^{3+}/(Na^+ + K^+)$ molar ratio; $\delta Eu = Eu_N/SQRT(Sm_N \times Gd_N)$; $\delta Ce = 2Ce_N/(La_N \times Pr_N)$. Symbol with "N" denotes the values normalised to chondrite (modified from [26]).

Table 4. Measured contents of major (wt. %), rare earth, and trace elements (ppm) of the Surrounding rock and Huanshan granite.

Sample	D54-YH1	D54-YH2	D54-YH3	D54-YH4	D54-YH5	D63-YH1	D63-YH2	D63-YH3	D63-YH4	D63-YH5
SiO_2	71.86	71.27	69.24	70.49	67.91	73.63	72.63	74.88	74.56	73.38
Al_2O_3	15.04	15.56	15.65	15.59	16.08	14.41	14.70	13.74	14.23	14.71
Fe_2O_3	1.48	1.61	1.80	1.95	2.09	0.88	1.01	0.66	0.75	0.95
FeO	0.44	0.43	0.71	0.50	0.72	0.58	0.62	0.43	0.39	0.54
CaO	1.89	2.13	3.18	2.56	3.63	0.99	1.04	0.96	0.82	1.04
MgO	0.61	0.47	0.89	0.53	1.01	0.30	0.32	0.25	0.22	0.26
K_2O	1.72	1.59	1.98	1.53	2.02	4.25	4.49	4.67	4.52	4.46
Na_2O	5.99	6.11	5.52	6.07	5.47	4.07	3.97	3.72	3.95	3.97
TiO_2	0.22	0.23	0.28	0.26	0.29	0.20	0.20	0.13	0.14	0.18
P_2O_5	0.06	0.06	0.08	0.07	0.09	0.06	0.07	0.04	0.05	0.06
MnO	0.03	0.03	0.04	0.05	0.05	0.06	0.06	0.04	0.04	0.05
LOI	0.23	0.16	0.33	0.11	0.36	0.30	0.61	0.29	0.09	0.12
Tatal	99.57	99.66	99.70	99.71	99.72	99.73	99.71	99.81	99.76	99.72
K_2O+Na_2O	7.71	7.70	7.50	7.60	7.49	8.32	8.46	8.39	8.47	8.43
A/CNK	1.0	1.0	0.9	1.0	0.9	1.1	1.1	1.1	1.1	1.1
A/NK	1.3	1.3	1.4	1.3	1.4	1.3	1.3	1.2	1.2	1.3
σ	2.1	2.1	2.1	2.1	2.3	2.3	2.4	2.2	2.3	2.3
R_1	2201	2146	2115	2111	2028	2421	2329	2542	2472	2391
R_2	380	404	538	453	596	262	271	250	238	268
Rb	62.2	42.7	69.7	53.1	73.8	208	201	174	201	214
Ba	2030	1400	1280	1070	1130	1480	1560	1040	1300	1520
Th	6.27	3.90	5.11	3.59	3.61	25.00	24.40	16.60	19.80	24.00
U	8.48	5.83	1.48	3.32	0.98	2.17	2.06	1.78	2.32	2.11
Ta	0.28	0.23	0.28	0.27	0.29	1.46	1.26	0.78	1.05	1.31
Nb	41.70	30.80	10.40	17.90	8.17	22.50	20.00	12.70	17.00	21.00
Pb	277.00	191.00	183.00	205.00	170.00	41.80	43.40	39.90	36.50	38.90
Sr	1530	1280	1020	1340	988	579	580	425	477	552
Zr	125.00	113.00	144.00	145.00	142.00	29.40	150.00	84.50	103.00	161.00
Hf	3.50	3.01	3.74	3.99	3.62	0.96	4.34	2.41	3.00	4.82
Y	23.00	29.10	30.00	15.60	28.50	11.50	10.80	6.06	6.80	9.95
Ga	18.3	16.7	20.9	19.7	20.1	21.8	21.0	16.8	18.7	20.8
La	49.60	23.10	31.60	20.80	24.50	33.30	25.20	15.60	19.80	23.50
Ce	75.80	34.20	46.80	35.20	40.10	83.20	67.00	43.80	50.20	65.20
Pr	8.25	4.06	5.44	3.85	4.86	7.75	6.10	3.66	4.57	5.64
Nd	26.90	13.10	16.90	12.50	14.40	24.50	19.20	11.40	14.30	18.10
Sm	4.06	1.96	2.44	1.95	2.27	3.95	3.36	1.93	2.36	3.15
Eu	1.36	0.71	0.84	0.67	0.81	1.00	0.90	0.58	0.70	0.89
Gd	2.67	1.47	1.79	1.42	1.81	2.94	2.46	1.45	1.73	2.38
Tb	0.38	0.20	0.24	0.21	0.26	0.41	0.35	0.23	0.27	0.32

 doi:10.20944/preprints202306.0870.v1

Dy	1.55	0.89	0.97	0.93	1.18	2.04	1.77	1.02	1.24	1.70
Ho	0.29	0.18	0.18	0.18	0.22	0.36	0.34	0.19	0.22	0.32
Er	0.74	0.48	0.52	0.49	0.62	1.03	1.00	0.55	0.62	0.89
Tm	0.11	0.07	0.08	0.08	0.10	0.15	0.14	0.09	0.10	0.14
Yb	0.68	0.46	0.45	0.48	0.62	0.96	0.97	0.55	0.61	0.90
Lu	0.10	0.07	0.07	0.07	0.10	0.15	0.14	0.09	0.09	0.14
REE	172.49	80.95	108.32	78.83	91.84	161.74	128.93	81.13	96.81	123.27
$LREE_N/HREE_N$	10.92	8.77	10.51	8.20	7.63	7.65	6.74	7.08	7.44	6.76
$(La/Yb)_N$	49.41	34.02	47.57	29.35	26.77	23.50	17.60	19.21	21.99	17.69
$(La/Sm)_N$	7.68	7.41	8.15	6.71	6.79	5.30	4.72	5.08	5.28	4.69
$(Gd/Yb)_N$	3.18	2.59	3.23	2.40	2.37	2.48	2.06	2.14	2.30	2.14
δEu	1.25	1.27	1.22	1.22	1.21	0.89	0.95	1.05	1.05	0.99
δCe	0.82	0.79	0.79	0.88	0.84	1.20	1.26	1.35	1.23	1.32
10000×Ga/Al	2.30	2.03	2.52	2.39	2.36	2.86	2.70	2.31	2.48	2.67

NOTE: Abbreviations- LREE: light rare earth element; HREE: heavy rareearth element; REE: rare-earth element; LOI: loss on ignition; $\sigma = (K_2O+Na_2O)^2/(SiO_2-43)$; $Mg^{\#} = Mg^{2+}/(Mg^{2+} + Fe^{2+})$ molar ratio; $R_1 = 4Si^{4+}-11 \times (Na^+ + K^+) - 2 \times (Fe^{3+} + Fe^{2+} + Ti^{4+})$ molar ratio; $R_2 = 6Ca^{2+} + 2Mg^{2+} + Al^{3+}$, molar ratio; $A/CNK = 2Al^{3+}/(Ca^{2+} + 2Na^+ + 2K^+)$ molar ratio; $A/NK = Al^{3+}/(Na^+ + K^+)$ molar ratio; $\delta Eu = Eu_N/SQRT(Sm_N \times Gd_N)$; $\delta Ce = 2Ce_N/(La_N \times Pr_N)$. Symbol with "N" denotes the values normalised to chondrite (modified from [26]).

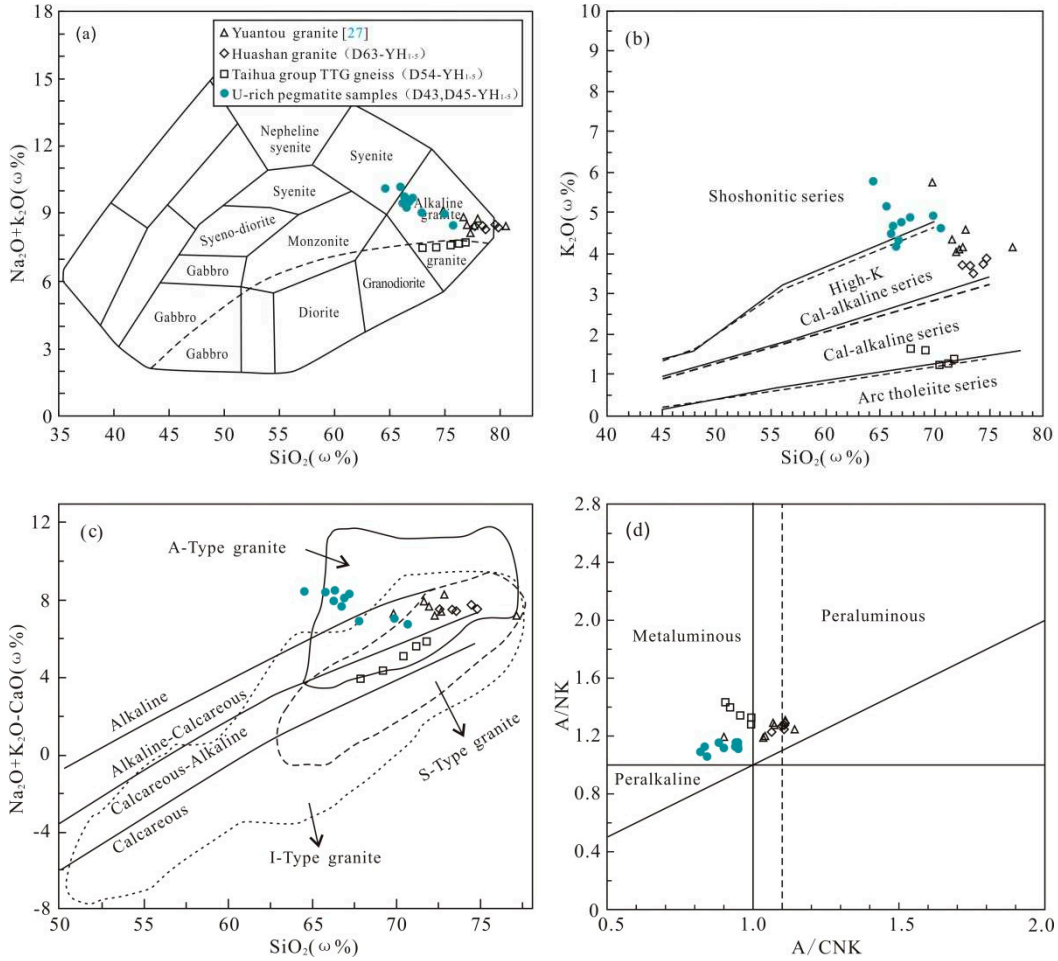

Figure 9. (a) SiO_2 vs.Na_2O+K_2O diagram; (b)SiO_2 vs.K_2O diagram (modified from [28]); (c)SiO_2 vs.Na_2O+K_2O-CaO diagram (modified from [29]); (d) A/CNK vs. A /NK diagram(modified from [29]).

 doi:10.20944/preprints202306.0870.v1

5.3. Trace Element Compositions

The content of rare earth elements (ΣREE) in the U-rich granitic pegmatite samples had a range from 430.50–1286.18×10^{-6} (Table 3), indicating that the REE in the U-rich granitic pegmatite had the characteristics of high total amount but very uneven distribution. In the chondrite-normalised diagrams (Figure 10a), all samples showed LREE-enriched and HREE depletion with $(La/Yb)_N$ =14.36–54.66. Meanwhile, the HREE exhibited a relatively flat patterns with $(Gd/Yb)_N$ =2.05–3.46 and weak negative Eu anomalies (δEu=0.57–1.19) (Figure 10a). Moreover, all of the U-rich granitic pegmatite samples were enriched in large-ion lithophile elements (such as Rb, Ba, K, and Pb) and radioactive elements (such as Th and U), and depleted in high field strength elements (such as Ta, P, Ti, Zr, and Hf) (Figure 10b). Obviously, the combination and enrichment characteristics of the trace elements in the U-rich granitic pegmatite samples were also consistent with the actual ore-forming elements(such as U,Nb,Pb, and REE). Compared with the Yuantou granite [27], Huashan granit and TTG gneiss of Taihua group, the U-rich granite pegmatite sample has a higher total amount of rare earth elements (Figure 10a), as well as Th, U, Pb and other trace element combinations (Figure 10b). This feature is also consistent with the actual metallogenic element combinations (such as U, Nb, Pb, REE, etc.) in this area.

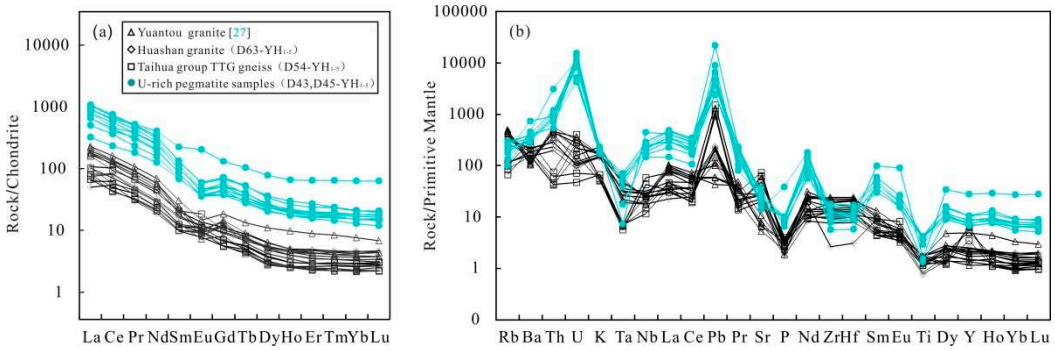

Figure 10. (a) Chondrite-normalised REE patterns; (b) Primitive mantle-normalised trace multi-element patterns (Chondrite and primitive mantle values are from [26]).

5.4. In Situ Zircon Hf Isotopic Compositions

Twenty zircon grains from the two groups of zircon samples were analysed for their Hf isotopic compositions. The results of the Lu–Hf analysis are presented in Table 5. These measured zircons have homogeneous Hf isotopic compositions and relatively high $^{176}Hf/^{177}Hf$ ratios (0.281359–0.281539), with depleted $\varepsilon_{Hf}(t)$ values varying from -19.42–-15.02 (Table 5, Figure 11a). Correspondingly, their single- (t_{DM1}) and two-stage (t_{DM2}) model ages ranged from 2.61 to 2.41 Ga and 3.10 to 2.76 Ga (Table 5, Figure 11b), respectively. The Hf isotope composition of the zircon indicates that the Late Palaeoproterozoic U-rich granitic pegmatite in Huayangchuan was probably formed by the reworking or remelting of crustal material from the Middle Archean to the Neoarchean.

Table 5. Hf isotope results of zircons from the U-rich granitic pegmatite.

Site number	Age (Ma)	$^{176}Yb/^{177}Hf$	$^{176}Lu/^{177}Hf$	$^{176}Hf/^{177}Hf$	±2σ	$f_{Lu/Hf}$	$\varepsilon_{Hf}(t)$	T_{DM1} (Ga)	T_{DM2} (Ga)
D43-Hf 1	1800	0.028578	0.000703	0.281458	0.000026	-0.98	-17.96	2.49	2.91
D43-Hf 2	1862	0.019464	0.000491	0.281447	0.000027	-0.99	-16.48	2.49	2.91
D43-Hf 6	1819	0.012029	0.000361	0.281430	0.000025	-0.99	-18.04	2.51	2.95
D43-Hf 9	1838	0.016209	0.000414	0.281464	0.000025	-0.99	-16.41	2.46	2.84
D43-Hf 10	1850	0.011812	0.000311	0.281407	0.000022	-0.99	-17.99	2.53	2.98
D43-Hf 12	1838	0.013678	0.000342	0.281413	0.000026	-0.99	-18.11	2.53	2.96
D43-Hf 21	1874	0.016944	0.000438	0.281359	0.000024	-0.99	-19.23	2.61	3.10

 doi:10.20944/preprints202306.0870.v1

D43-Hf 23	1808	0.017472	0.000438	0.281431	0.000024	-0.99	-18.38	2.51	2.93
D43-Hf 25	1832	0.017730	0.000468	0.281436	0.000024	-0.99	-17.61	2.50	2.90
D43-Hf 29	1808	0.040893	0.000984	0.281420	0.000027	-0.97	-19.42	2.56	2.99
D45-Hf 8	1828	0.022944	0.000590	0.281423	0.000020	-0.98	-18.34	2.53	2.96
D45-Hf 9	1837	0.027094	0.000690	0.281484	0.000022	-0.98	-16.04	2.45	2.83
D45-Hf 10	1845	0.031770	0.000795	0.281511	0.000023	-0.98	-15.02	2.42	2.77
D45-Hf 11	1860	0.011456	0.000315	0.281452	0.000019	-0.99	-16.12	2.47	2.85
D45-Hf 12	1824	0.008961	0.000246	0.281485	0.000019	-0.99	-15.79	2.42	2.80
D45-Hf 13	1857	0.018569	0.000512	0.281492	0.000019	-0.98	-15.03	2.43	2.78
D45-Hf 14	1850	0.035348	0.000940	0.281490	0.000019	-0.97	-15.83	2.46	2.83
D45-Hf 26	1808	0.046560	0.001192	0.281539	0.000022	-0.96	-15.47	2.41	2.76
D45-Hf 27	1788	0.024690	0.000661	0.281465	0.000021	-0.98	-17.95	2.48	2.90
D45-Hf 30	1841	0.078297	0.002007	0.281534	0.000025	-0.94	-15.82	2.47	2.82

NOTE: $\varepsilon_{Hf}(t) = ((^{176}Hf/^{177}Hf)_S - (^{176}Lu/^{177}Hf)_S \times (e^{\lambda t}-1))/((^{176}Hf/^{177}Hf)_{CHUR,0} - (^{176}Lu/^{177}Hf)_{CHUR} \times (e^{\lambda t}-1)) - 1) \times 10{,}000$; $t_{DM1}(Ma) = 1/\lambda \times \ln(1+((^{176}Hf/^{177}Hf)_S-(^{176}Hf/^{177}Hf)_{DM})/((^{176}Lu/^{177}Hf)_S-(^{176}Lu/^{177}Hf)_{DM}))$; $t_{DM2}(Ma) = t_{DM1}-(t_{DM1}-t)((f_{CC}-f_S)/(f_{CC}-f_{DM}))$; $f_{Lu/Hf} = (^{176}Lu/^{177}Hf)_S/(^{176}Lu/^{177}Hf)_{CHUR}-1$; f_{CC}, f_S, and f_{DM} are $f_{Lu/Hf}$ values of continental crust, zircon samples and depleted mantle, respectively. Subscript with "S" denotes zircon samples analysed. Subscript with "CHUR" denotes Chondrite standard library. Subscript with "DM" denotes depleted mantle. $(^{176}Lu/^{177}Hf)_{CHUR} = 0.0332$; $(^{176}Hf/^{177}Hf)_{CHUR,0} = 0.282772$; $(^{176}Lu/^{177}Hf)_{DM} = 0.0384$; $(^{176}Hf/^{177}Hf)_{DM} = 0.28325$; $\lambda = 1.865 \times 10^{-11} ar^{-1}$.

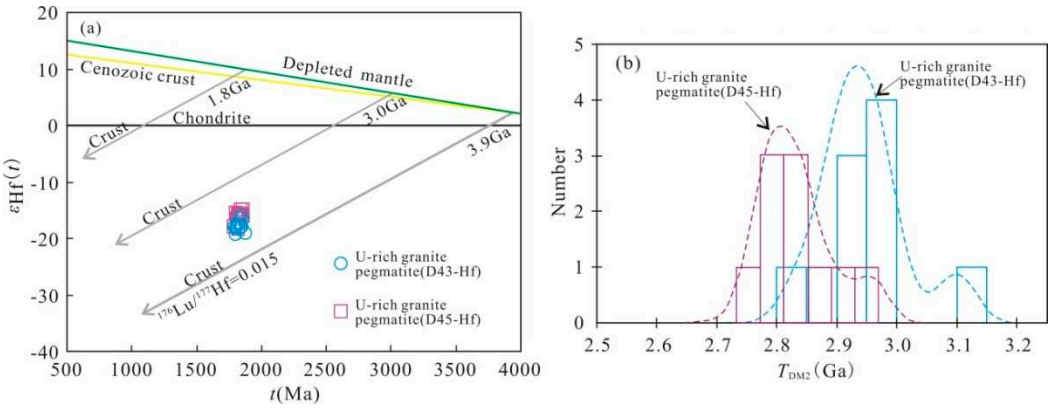

Figure 11. (a) $\varepsilon_{Hf}(t)$ vs. t (Ma) diagram of zircons; (b) T_{DM2} diagram of of zircons.

6. Discussion

6.1. Constraints from zircon age of Paleoproterozoic U mineralization

Based on field observations, the U-rich granitic pegmatite intruded into the Taihua Group in a large single vein, and the intrusive contact boundary with the Taihua Group was clearly visible (Figure 3a,b), showing the characteristics of magmatic rock intrusion. The CL images of zircons from U-rich granitic pegmatite samples also showed general characteristics of magmatic zircons [24]. The REE characteristics of the zircons were consistent with those of typical magmatic zircons (Figure 7a,c).

 doi:10.20944/preprints202306.0870.v1

The highly positive correlation of U and Th in zircon showed the characteristics of magmatic genesis (Figure 7b,d), reflecting that the zircon isotope system was still well sealed without the migration of U and Th. Under the polarising and scanning electron microscopes, zircon grains displayed an intact crystal form (Figure 3c, Figure 5e,f) and an association with uraninite (Figure 5f). Combined with the massive occurrence of betafites in the intergranular fissures of rock-forming minerals (Figure 5a–d), we speculate that the zircons had mineralisation characteristics in the diagenetic stage. Therefore, the zircon U–Pb dating results obtained in this study were 1826.3 ± 7.9 and 1829 ± 11 Ma (Figure 8b,d), which not only indicated the diagenetic age of U-rich pegmatite but also represented the age of uranium mineralisation in the same period.

Generally, orogenic belts on the margins of ancient continental blocks are important uranium metallogenic regions. First, ancient land blocks are often rich in large-ion lithophilic elements (e.g., Rb, Ba, Th, U, and K), which can easily provide material sources for uranium polymetallic mineralisation. Second, the crust and mantle materials on the margin of the ancient continental region have strong material interactions and frequent magmatic activities, which can create favourable geological conditions for the large-scale enrichment of ore-forming materials. Therefore, the marginal zone of the ancient continent often had favourable uranium polymetallic mineralisation conditions that controlled the temporal and spatial distribution of uranium polymetallic deposits [30,31]. Regionally, a large number of late Palaeoproterozoic (2.0–1.8 Ga) uranium polymetallic deposits are distributed along the collisional orogenic belt along the marginal zone of the ancient continental North China Craton. Typical deposits include the Lianshanguan uranium deposit in the Liaoning Province, the Pinglu uranium deposit in the Shanxi Province, and the Hongshiquan uranium deposit in the Gansu Province [30,31]. In conclusion, the chronological research results of U-rich granitic pegmatite in this study show that uranium mineralisation in the late Palaeoproterozoic (1829 ± 11 and 1826 ± 7.9 Ma) also occurred in the Xiaoqinling area of the southern margin of the North China Craton, which implies that the tectonic–magmatic–mineralization events were produced during the ultimate cratonisation process of the North China Craton in the late Palaeoproterozoic (2.0–1.8 Ga) [32–34].

6.2. Rock Type of U-rich granitic pegmatite

Lithologically, A-type granites can be further divided into peralkaline and aluminous types [35]. Peralkaline A-type granite with a high degree of magmatic differentiation was formed during the latest time series of magmatic activity. They are often associated with iron–magnesia rocks (such as mafic inclusions, xenoliths, and intrusive veins) and often contain alkaline dark minerals (such as aegirine, aegirine–augite, sodium amphibole, sodium iron amphibole, and olivine) [36]. The peralkaline A-type granite is characterised by high SiO_2, rich total alkalis (K_2O+Na_2O), and relatively poor MgO and low CaO; they usually enrich large-ion lithophile elements (LILEs: such as Rb, Th, U, and K), and depletion of high field strength elements (HFSEs: such as Zr, Nb, Ta, and Ti) [37]. Their ΣREEs are usually several times or even dozens of times greater than that of other types of granites and they have strong negative δEu anomalies in the chondrite-normalised diagrams [38]. They usually also have high K_2O/Na_2O values, A/CNK ratios >1, and 10000 × Ga/Al ratios >2.6. Compared to peralkaline A-type granites, aluminous A-type granites have a relatively low degree of magmatic differentiation [39], therefore, they also show slightly different mineral and geochemical characteristics. The aluminous A-type granite is relatively rich in aluminium (Al_2O_3 >12 wt.%), but the A/CNK and 10000 × Ga/Al value are relatively low. They have a high content of light REE, thus showing more obvious characteristics of light and heavy rare earth fractionation, butδEu is usually not obvious [38]; The dark minerals of aluminous A-type granites are mainly ordinary hornblende or biotite [40].

The U-rich granitic pegmatite samples in this study were characterised by high SiO_2 (64.37–70.69 wt.%) , total alkali values (K_2O + Na_2O = 8.50–10.30 wt.%), and Al_2O_3 (12.20–14.41 wt.%)， and relatively low Ti_2O (0.23–0.73 wt.%), MgO (0.38–0.90 wt.%), P_2O_5 (0.14–0.83 wt.%), and MnO (0.04–0.57 wt.%). Most of the U-rich granitic pegmatite samples belonged to the A-type granite in the SiO_2 vs. Na_2O+K_2O-CaO diagram and showed alkaline and alkaline calcareous series (Figure 9c). The

 doi:10.20944/preprints202306.0870.v1

A/CNK values of these samples had a range from 0.8 to 0.9 (Table 3), and most of them were metaluminous (Figure 9d) in the A/CNK vs. A/NK diagram; The 10000 × Ga/Al ratios of the samples were 2.83–3.99 (average = 3.41) (Table 3), and most of them fell into the range of A-type granite in the 10000 × Ga/Al vs. (K_2O+Na_2O) diagram (Figure 12a), 10000 × Ga/Al vs.Y diagram (Figure 12b), 10000 × Ga/Al vs. (Na_2O + K_2O)/CaO diagram (Figure 12c) and Zr+Nb+Ce+Y vs. (Na_2O + K_2O)/ CaO diagram (Figure 12d), which also shows different rock type characteristics from the Huashan granite and TTG of Taihua group. The trace elements of the U-rich granitic pegmatite samples also showed enrichment of large-ion lithophile elements (typically Rb, Ba, K, and Pb) and radioactive elements (such as Th and U), and depletion of high-field strength elements (such as Ta, Nb, P, Ti, and Hf (Figure 10b). The U-rich granitic pegmatite samples also have a high total content of rare earth elements (ΣREE), but fractionation characteristics of LREE and HREE are obvious, and negative δEu anomalies are relatively weak (Figure 10a). No dark alkaline minerals were observed in the U-rich granitic pegmatite samples (Figure 4). In summary, the U-rich granitic pegmatites of the late Palaeoproterozoic in the Huayangchuan deposit were equivalent to aluminous A-type granites.

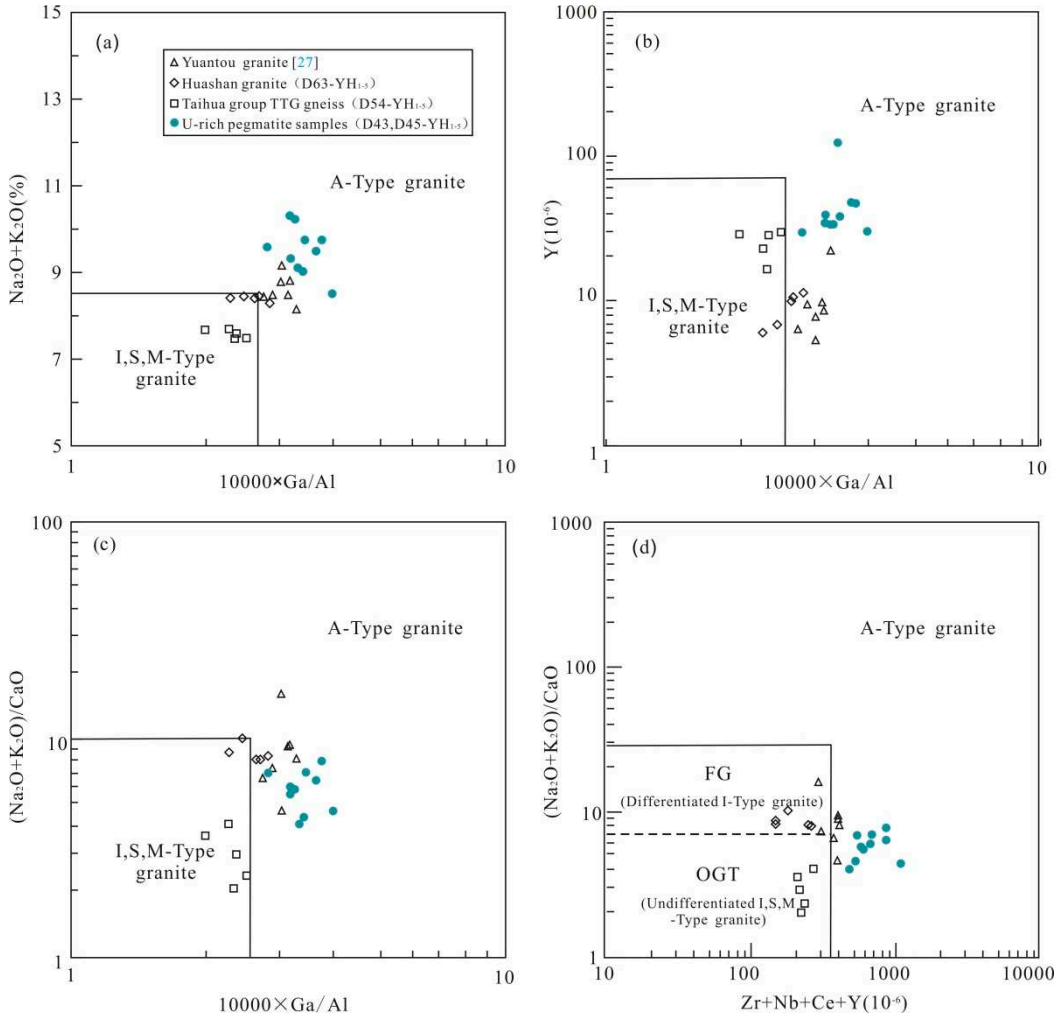

Figure 12. (a) 10000 × Ga/Al vs. Na_2O + K_2O diagram; (b) 10000 × Ga/Al vs.Y diagram; (c) 10000 × Ga/Al vs. (Na_2O + K_2O)/ CaO diagram ; (d) Zr+Nb+Ce+Y vs. (Na_2O + K_2O)/ CaO diagram (modified from [37]).

6.3. Tectonic Setting of U mineralization

Type A granites are generally formed in tensile or extensional tectonic settings [36]. The tectonic settings of A-type granites can be divided into non-orogenic and post-orogenic types [41]. Globally, A-type granites were very rare before the Palaeoproterozoic but began to appear in large quantities

 doi:10.20944/preprints202306.0870.v1

during the late Palaeoproterozoic (early Mesoproterozoic) [42]. This phenomenon implies a transition of the tectonic system from compression to extension during the continental evolution [43]. During the late Palaeoproterozoic (2.0–1.8 Ga), all kinds of rocks in the basement of the North China Craton underwent strong metamorphism and deformation [44]. This process lasted at least 150 Ma, which was the widespread land–land collision events, and this tectonic event was known as the Luliang movement [45]. The Luliang movement promoted a unified crystalline basement in the North China Craton. A series of magmatic activities occurred in the North China Craton after the Luliang movement. For example, Yang (2020) [46] obtained zircon U–Pb ages of felsic pegmatite, granodiorite, and monzogranite in the Xiaoqinling area on the southern margin of the North China Craton, which were aged approximately 1926, 1808, and 1807 Ma, respectively, reflecting tectonic magmatism after the end of the Luliang movement. Thereafter, the bimodal volcanic rocks of Xiong'er group (1.80–1.75 Ga) [47], the volcanic–sedimentary formation of Changcheng group (1.68–1.62 Ga) [48], and the contemporaneous or later (1.72–1.60 Ga) basic dyke swarms [49], all these indicate that the Xiaoqinling area on the southern margin of the North China Craton had been in a continuous regional extensional environment since the Luliang movement.

In the SiO_2 vs. lg[Ca/(Na_2O + K_2O)] diagram(Figure 13a)and R_1 vs. R_2 diagram(Figure 13b), most of the U-rich granitic pegmatite samples plotted in a extensional and non-orogenic tectonic setting. In the Y vs. Nb diagram(Figure 14a), Yb vs. Ta diagram(Figure 14b), Y+Nb vs. Rb diagram(Figure 14c) and Yb+Ta vs. Rb diagram(Figure 14d), most of the U-rich granitic pegmatite samples are generally in an intra-plate granite tectonic setting (WPG) [50]. In the Y-Nb-3×Ga diagram(Figure 15a), Y-Nb-3×Ce diagram(Figure 15b) and Yb+Ta vs. Rb diagram(Figure 15d), most of the U-rich granitic pegmatite samples belong to intraplate A_1-type granite [36]. Therefore, the above results indicate that the Xiaoqinling belt in the southern margin of the North China Craton was already in a non-orogenic extensional setting when the U-rich granitic pegmatites were formed (1826.3 ± 7.9 and 1829 ± 11 Ma). The reconstruction scheme of the Columbia supercontinent in the late Paleoproterozoic (2.0–1.8 Ga) provided the location of the North China Craton. At this time, the southern margin of the North China Craton was located in the intraplate rift zone of the Colombian supercontinent [51], which had the non-orogenic tectonic conditions of a plate margin or intraplate rift.

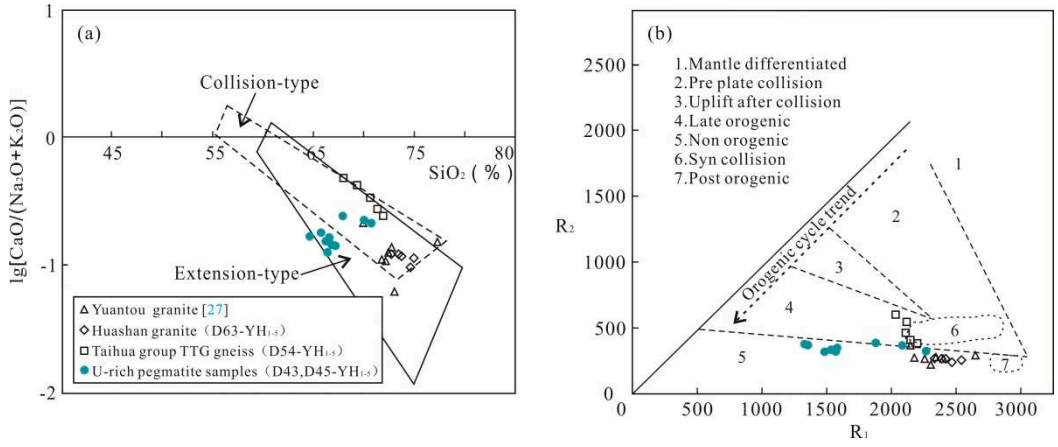

Figure 13. (a)SiO_2 vs. lg[Ca/(Na_2O + K_2O)] diagram (modified from [52]); (b)R_1 vs. R_2 diagram (modified from [53]).

 doi:10.20944/preprints202306.0870.v1

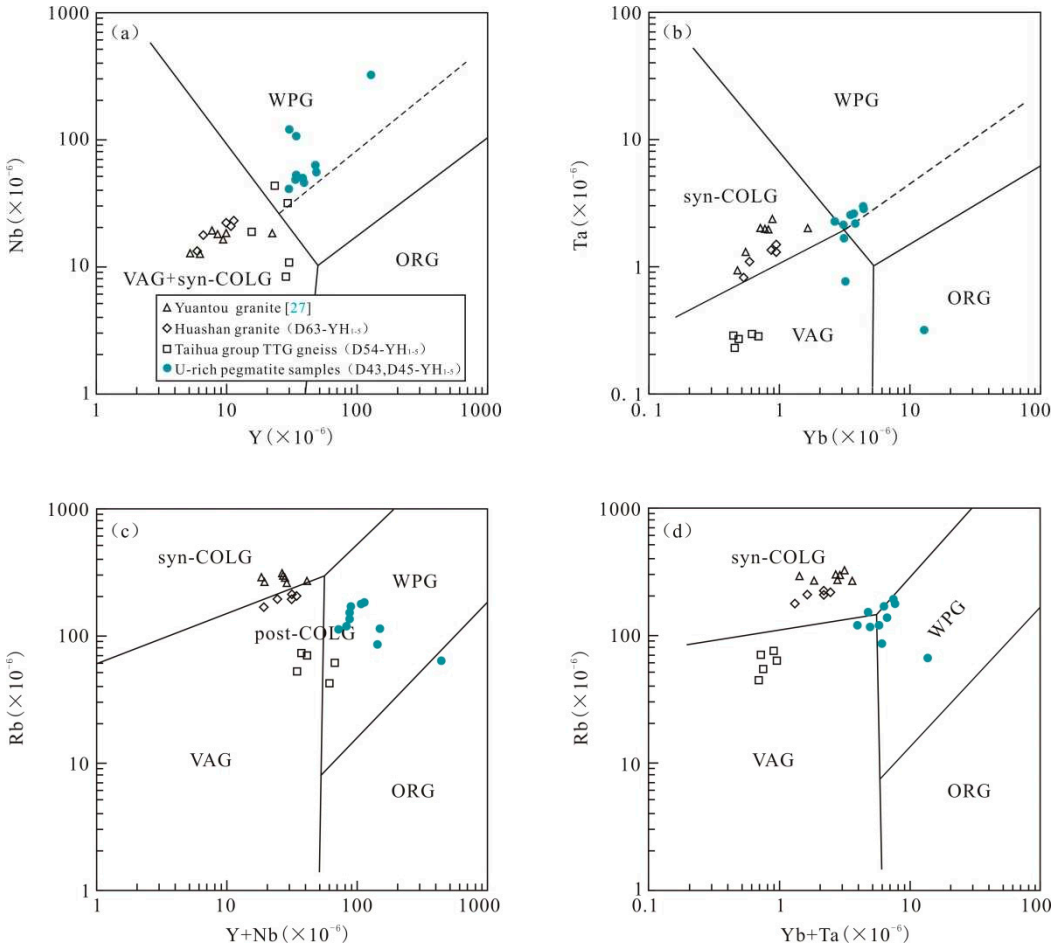

Figure 14. (a) Y vs. Nb diagram; (b) Yb vs. Ta diagram; (c) Y+Nb vs. Rb diagram; (d) Yb+Ta vs. Rb diagram (modified from [50]).

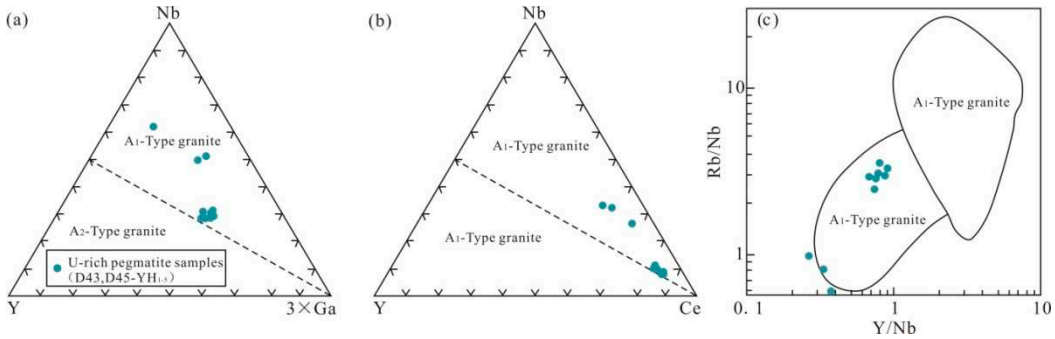

Figure 15. (a) Y-Nb- 3×Ga diagram; (b)Y-Nb- 3×Ce diagram; (c)Y/Nb vs. Rb/Nb diagram (modified from [36]).

6.4. Rock and mineralisation genesis of U-rich granitic pegmatite

Currently, there are four viewpoints on the genetic model of A-type granite: first, the crustal rocks are partially melted to form I-type granite, and then the residual materials are partially melted again to form A-type granite [54]; however, experimental petrology and actual observations proved that the residual crustal material cannot differentiate A-type granite [55]. Second, A-type granite is formed by the partial melting of the crystalline basement or metamorphic sedimentary rocks [35]. Third, A-type granite is formed by crust–mantle magmatic mixing [56]. Fourth, the separation crystallisation of mantle-derived alkaline basalt directly forms A-type granite [57]. The studied U-rich granitic pegmatite samples have the characteristics of high SiO_2, Al_2O_3, and total alkalis, low MgO, TiO_2, and P_2O_5, and enrichment in large-ion lithophiles and radioactive elements (such as Rb,

 doi:10.20944/preprints202306.0870.v1

Ba, Th, U, K, and Pb) and depletion of high-field-strength elements (such as Ta, Nb, P, Ti, and Hf). These whole-rock geochemical characteristics support the conclusion that the magma source of the U-rich granitic pegmatite samples was felsic crustal material, rather than mantle-derived mafic magma. In addition, experimental petrology has proved that felsic rocks in the shallow crust (depth ≤20 km) can produce A-type granites melt through dehydration, high temperature, and partial melting [58]. In fact, the lithology of Taihua Group as the basement were composed of "supracrustal rock" and "TTG suite" (Trondhjemite, Tonalite, and Granodiorite), whose material composition clearly belongs to the evolved felsic crust. The formation ages of Taihua Group were approximately 2.8, 2.5, 2.3 and 1.97–1.8 Ga [32,34,59], reflecting the multi-stage cyclic evolution of the crust in this area. The formation age of the early Taihua Group (approximately 2.8 Ga) is much older than that of the later U-rich granitic pegmatite and is very close to the two-stage model age (T_{DM2}) of the zircon Hf isotope (3.10–2.76 Ga). This evidence indicates that the materials of the early Taihua Group (such as the Middle Archean) were probably the magma source of the later Taihua Group (such as the Late Palaeoproterozoic).

Therefore, we can speculate that the formation process of U-rich granitic pegmatite in this study was as follows: after the Late Palaeoproterozoic (1826.3 ± 7.9 and 1829 ± 11 Ma) Luliang movement, the tectonic setting in this area gradually transitioned to an extensional background [27]. The subduction plates broke off and triggered asthenospheric mantle upwelling, resulting in partial melting of the lithospheric mantle, and the generated basic magma rose and underplated the middle-lower crust, prompting partial melting of the early Taihua Group formed in the Archean-Neoarchean (3.10–2.76 Ga). As extension continued, a series of A-type granites gradually formed, such as in the Yuantou and Huayangchuan areas (Figure 16a). The Taihua Group formed in the Archean-Neoarchean was rich in uranium and other radioactive elements, and the uranium-rich granitic pegmatites in this area were directly formed during the magmatic activity in the late Palaeoproterozoic (1826.3 ± 7.9 and 1829 ± 11 Ma) (Figure 16b). These U-rich granitic pegmatites also provided material sources for later (Indosinian and Yanshanian) uranium mineralisation in the Huayangchuan area or underwent superimposed transformation to form new deposit types, reflecting the ultra-long evolutionary history of uranium mineralisation and uranium deposits with complex genesis in the Huayangchuan area.

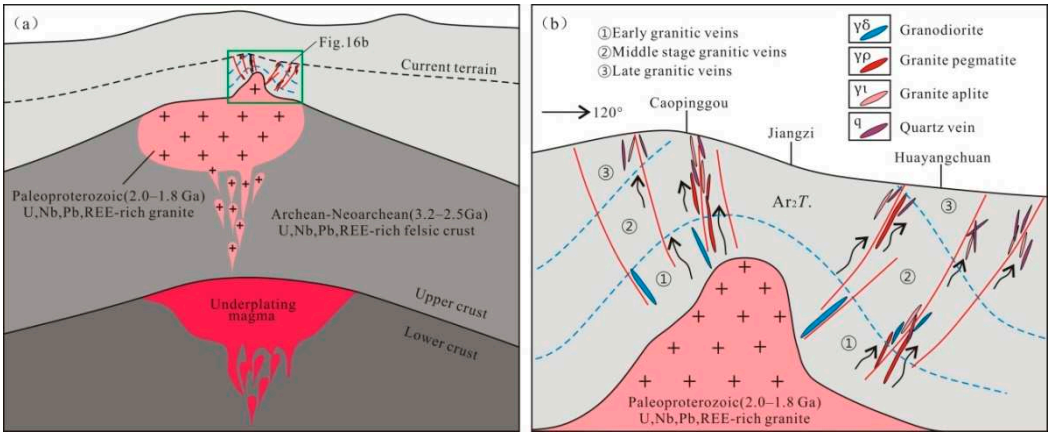

Figure 16. (a) Rock genesis pattern drawings of Paleoproterozoic U-rich granitic pegmatite; (b)Mineralisation genesis pattern drawings of Paleoproterozoic U-rich granitic pegmatite.

7. Conclusion

1. The U-rich granitic pegmatites were formed in the late Palaeoproterozoic (1826.3 ± 7.9 and 1829 ± 11 Ma). The symbiotic phenomena of the magmatic zircons with betafite and uraninite in the samples showed metallogenic characteristics during the diagenetic period.
2. Based on the classification criteria and rock characteristics of A-type granite, the major elements, trace elements, and mineral compositions of most U-rich granitic pegmatite samples had the characteristics of intraplate A_1-type granite

3. The U-rich granitic pegmatites were formed after the Luliang movement in the late Palaeoproterozoic, and the tectonic system gradually transitioned from a continent–continent collision to an extensional setting. The partial melting of the early Taihua Group materials formed in the Archean-Neoarchean triggered a series of tectonic granitic magmatic activities.
4. The early Taihua Group formed in the Archean-Neoarchean as mature crust material rich in uranium, which provided uranium-rich magma for the formation of uranium-rich granite pegmatite in the late Palaeoproterozoic. Existing uranium-rich geological bodies also provided material sources for later uranium mineralisation in the Huayangchuan deposit.

Author Contributions: Putao Li — — Conceptualization, Methodology, Formal analysis, Investigation, Resources, Data curation, writing- original draft, Writing-review & editing, Visualization. Yongjun Li—— Writing-review & editing, Supervision. Pingyang Gu——Investigation, Resources, Data curation, Project administration. Shiping He——Investigation, Data curation. Yujun Zhuang——Investigation, Data curation. Ruiming Chen——Investigation, Data curation.

Funding: This research was financially supported by the Geological Survey Project of the China Geological Survey (Grant No. DD20160014, DD20190069, and DD20221636).

Institutional Review Board Statement: Not applicable.

Informed Consent Statement: Not applicable.

Data Availability Statement: Data is contained within the article.

Acknowledgments: We are very grateful to Qingqing Kang, Peng Li, Lei Li, and Hongjun Jiang of Geological Party No. 224, Sino Shaanxi Nuclear Industry Group, for their assistance in the field sampling work, and the reviewers for their constructive comments and suggestions which improved the quality of the manuscript.

Conflicts of Interest: There is no conflict of interest for this work.

References

1. He, S.; Li, Z.Y.; Hui, X.C.; Guo, J. $^{40}Ar/^{39}Ar$ geochronology of biotite in Huayangchuan uranium-polymetallic deposit in shaanxi province and its geological significance. Uranium Geology. 2016, 32(3), 159-164 (in Chinese with English abstract).
2. Gao, C.; Kang, Q.Q.; Jiang, H.J.; Li, P.; Zhang, X.M.; Li, L.; Dong, Q.Q.; Ye, X.C.; Hu, X.J. A unique uranium polymetallic deposit discovered in the Qinlingorogenic belt:The Huayangchuan super-large U-Nb-Pb-REE deposit associated with pegmatites and carbonatites. Geochimica. 2017, 46(5), 446-455 (in Chinese with English abstract).
3. Kang, Q.Q.; Zhang, X.M.; Meng, X.H. Analysis on the characteristics and prospecting of rare earth ore in the western section of Xiaoqinlin. Northwestern Geology. 2020, 53(1), 107-121 (in Chinese with English abstract).
4. Li, N.; Chen, Y.J.; Zhang, H.; Zhao, T.P.; Deng, X.H.; Wang, Y.; Ni, Z.Y. Molybdenum deposits in East Qinling. Earth Science Frontiers. 2007, 14(5), 186-198 (in Chinese with English abstract).
5. Wang, L.J.; Xu, C.; Wu, M.; Song, W.L. A study of fluid inclusion from Huayangchuan carbonatite. Acta Mineralogical Sinica. 2011, 31(3), 374-375 (in Chinese with English abstract).
6. Hui, X.C.; Cai, Y.Q.; He, S.; Feng, Z.S. Petrologic and geochemical characteristics of carbonatites in Huayangchuan U-Nb-Pb deposit, Shaanxi province. Geoscince. 2017, 31(2), 246-257 (in Chinese with English abstract).
7. Yu X.H. Geological, petrol-mineralogical characteristics and origin of the carbonatites from Huayangchuan, Shaanxi province. Earth Science-Journal of China University of Geosciences. 1992, 17(2): 151-158 (in Chinese with English abstract)
8. Xu, C.; Campbell, I.H.; Allen, C.M.; Huang, Z.; Qi, L.; Zhang, H.; Zhang, G. Flat rare earth element patterns as an indicator of cumulate processes in the Lesser Qinling carbonatites, China. Lithos. 2007, 95, 267-278.
9. Reguir, E.P.; Chakhmouradian, A.R.; Pisiak, L.; Halden, N.M.; Yang, P.; Xu, C.; Kynický, J.; Cou€eslan, C.G. Trace-element composition and zoning in clinopyroxene- and amphibole-group minerals: implications for element partitioning and evolution of carbonatites. Lithos. 2012, 128, 27-45.
10. Hui, X.C.; He, S. Mineralization characteristic of carbonatite veins in Huayangchuan U-polymetal deposit, Shaanxi province. Uranium Geol. 2016, 32,93-98 (in Chinese with English abstract).

11. Song, W.L.; Xu, C.; Smith, M.P.; Kynicky, J.; Huang, K.J.; Wei, C.W.; Zhou, L.; Shu, Q.H. Origin of unusual HREE-Mo-rich carbonatites in the Qinling orogen, China. Science Reports. 2016, 6,1-10.
12. Gao, L.G.; Chen, Y.W.; Bi, X.W.; Hu, R.Z.; Gao, C.; Dong, S.H.; Luo J.C. Chronology and mineral chemistry of the uranium minerals in Huayangchuan uranium-niobium deposit. Shaanxi province and its implications for uranium mineralization. Acta Geologica Sinica. 2019, 93(9), 2273-2291 (in Chinese with English abstract).
13. Jiang, H.J.; Gao, C.; Kang, Q.Q.; Chen, H.Y.; Zheng, H.; Chen, B.; Dong, Q.Q.; Zhang, X.M.; Li, P.; Li, Liu, K.H.; He, S.P. Mineralization paragenesis of Huayangchuan U-Nb-Pb deposit in the Lesser Qinling. Geotectonica et Metallogenia. 2020, 44(3), 404-421 (in Chinese with English abstract).
14. Meng, Q.R.; Zhang, G.W. Timing of collision of the North and South China blocks: Controversy and reconciliation. Geology. 1999, 27, 123-126.
15. Li, Y.F.; Wang, C.Q.; Bai, F.J.; Song, Y.L. Re-Os isotopic ages of Mo deposit in east Qinling and their geodynamic settings. Miner. Resour. Geol. 2004, 6,571-578 (in Chinese with English abstract).
16. Ludwig, K. R. User's manual for Isoplot 3.0: a geochronological toolkit for Microsoft Excel. Berkeley Geochronology Center Special Publication, p. 2003, 1-71.
17. Andersen, T. Correction of common lead in U-Pb analysis that do not report ^{204}Pb. Chemical Geology. 2002, 192, 59-79. https://doi.org/10.1016/S0009-2541(02)00195-X.
18. Yang, G.X.; Li, Y.J.; Xiao, W.J.; Tong, L.L. OIB-type rocks within West Junggar ophiolitic melanges: Evidence for the accretion of seamounts: Earth-Science Reviews. 2015, 150, 477-496. doi: 10.1016/j.earscirev.2015.09.002.
19. Hou, K.J.; Li, Y.H.; Zou, T.R.; Qu, X.M.; Shi, Y.R.; Xie, G.Q. LA-MC-ICP-MS technique for Hf isotope microanalysis of zircon and its geological applications. Acta Petrologiea Sinica. 2007, 23(10), 2595-2604 (in Chinese with English abstract).
20. Blichert-Toft, J.; Albarède, F. The Lu-Hf isotope geochemistry of chondrites and the evolution of the mantle-crust system: Earth and Planetary Science Letters. 1997, 148, 243-258. doi: 10.1016/S0012-821X(97)00040-X.
21. Scherer, E.; Münker, C.; Mezger, K. Calibration of the lutetium-hafnium clock: Science. 2001, 293, 683-687. doi: 10.1126/science.1061372.
22. Griffin, W.L.; Pearson, N.J.; Belousova, E.; Jackson, S.E.; Van Achterbergh, E.; O'Reilly, S.Y.; Shee, S.R. The Hf isotope composition of cratonic mantle: LAM–MC–ICPMS analysis of zircon megacrysts in kimberlites: Geochimica et cosmochimica acta, v. 64, p. 2000, 133-147. doi: 10.1016/S0016- 7037(99)00343-9.
23. Diwu, C.R.; Sun, Y.; Dong, Z.C.; Wang, H.L.; Chen, D.L.; Chen, L.; Zhang, H. In situ U-Pb geochronology of Hadean zircon xenocryst(4.1-3.9 Ga) from the western of the Northern Qinlinig orogenic belt. Acta Petrologica Sinica. 2010, 26(4), 1171-1174 (in Chinese with English abstract).
24. Rubatto, D. Zircon trace element geochemistry: Partitioning with garnet and the link between U-Pb ages and metamorphism. Chemical Geology. 2002, 184, 123-138.
25. Xu, Q.; Li, Y.; Yang, G.X.; Ning, W.T.; Tong,L.L.; Duan,F.H.; Wu, L.; Ren, P.F. Petrogenesis and tectonic setting of the Middle Devonian Beitashan Formation volcanic rocks in the northern East Junggar, NW China: Insights from geochemistry, zircon U–Pb dating, and Hf isotopes. Geological Journal. 2020, 55, 1964-1983. https://doi. org/10.1002/gj.368.
26. Sun, S.S.; McDonough, W.F. Chemical and isotopic systematic of oceanic basalt: Implications for mantle compositions and processes. Geological Society, London, Special Publications. 1989, 42, 313-345. doi: 10.1144/GSL.SP.1989. 042.01.19.
27. Deng, X.Q.; Peng, T.P.; Zhao, T.P.; Qiu, Z.L. Petrogenesis of the Late Paleoproterozoic (-1.84 Ga) Yuantou A-type granite in the southern margin of the North China Craton and its tectonic implications. Acta Petrologica Sinica. 2019, 35(8), 2455-2469, (in Chinese with English abstract).
28. Irvine, T.N.; Baragar, W.R.A. A guide to the chemical classification of the common volcanic rocks: Canadian Journal of Earth Sciences, v. 8, p. 1971, 523-548. doi: 10.1139/ e71-055.
29. Wilson, M. Igneous Petrogenesis: A Global Tectonic Approach. London: Chapman & Hall. 1989, 13-34.
30. Wang, W.G.; Wang, J., 1991. The unique economic uranium mineral assemblage in Lianshanguanuranium deposit and its chatacteristics and significance. Uranium Geology 7(4), 196-205 (in Chinese with English abstract).
31. Song, J.Y.; Cai, Y.Q.; Yao, C.L.; Zhu.; P.F.; Zhao., Y.A.; Zhang, W.M. The relationship between Paleo-Landmass and uranium mineralization in China. Uranium Geology. 2011, 27(1), 8-12 (in Chinese with English abstract).

32. Wan, Y.S.; Wilde, S.A.; Liu, D.Y.; Yang, C.X.; Song, B.; Yin, X.Y., 2006. Further evidence for -1.85Ga metamorphism in the central zone of the north China Craton:SHRIMP U-Pb dating of zircon frommetamorphic rocks in the Lushan area, Henan province. Gondwana Research 9(1-2), 189-197.
33. Xia, Y.L.; Han, J., 2008. Uranium ore-forming ages of the oldest uranium deposits in China and the tracing of uranium metallogenic provinces with lead isotopes. Acta Geoscientica Sinica 29(6), 752-760 (in Chinese with English abstract).
34. Liu, D.Y.; Wilde, S.A.; Wan, Y.S.; Wang, S.Y.; Valley, J.W.; Kita, N.; Dong, C.Y.; Xie, H.Q.; Yang, C.X.; Zhang, Y.X.; Gao, L.Z. Combined U-Pb, Hafnium and Oxygen isotope analysis of zircons from meta-igneousrocks in the southern north China craton reveal multiple events inthelate Mesoarchean-early Neoarchean. Chemical Geology. 2009, 261(1-2), 140-154.
35. Zhou, Y.Y.; Zhai, M.G.; Zhao, T.P.; Lan, Z.W.; Sun Q.Y. Geochronological and geochemical constraints on the petrogenesis of the Early Paleoproterozoic potassic granite in the Lushan area, southern margin of the North China Craton. Journal of Asian Earth Sciences. 2014, 94, 190-204.
36. Eby, G.N. Chemical subdivision of the A-type granitoids: Petrogenetic and tectonic implications. Geology. 1992, 20(7), 641-644.
37. Whalen, J.B.; Currie, K.L.; Chappell, B.W. A-type granites: Geochemical characteristics, discrimination and petrogenesis. Contributions to Mineralogy and Petrology. 1987, 95(4), 407-419.
38. Wu,S.P.; Wang, M.Y.; QI, K.J. Present situation of researches on A-type granites: a review. Acta Petrologica Et Mineralogica. 2007, 26(1),57-66 (in Chinese with English abstract).
39. King, P.L.; White, A.J.R.; Chappell, B.W.; Allen, C.M. Characterization and origin of aluminous A-type granites from the Lachlan Fold Belt, southeastern Australia. Journal of Petrology. 1997, 38(3), 371-391.
40. Wu, F.Y.; Sun, D.Y.; Li, H.M.; Jahn, B.M.; Wilde, S. A-type granites in northeastern China: Age and geochemical constraints on their petrogenesis. Chemical Geology. 2002, 187(1-2), 143-173.
41. Xu, B.L.; Yan, G.H.; Zhang, C., 1998. Prtrological subdivision and source material of A-type granites. Earth Science Frontiers 5(3), 113-124 (in Chinese with English abstract).
42. Dall'Agnol, R.; Frost, C.D.; Rm, O.T. IGCP Project 510"A-typegranites and related rocks through time": Project vita, results, and contribution to granite research. Lithos. 2012, 151, 1-16.
43. Zhai, M.G.; Santosh, M.; Zhang, L.C. Precambrian geology and tectonic evolution of the North China Craton. Gondwana Research. 2011, 20(1), 1-5.
44. Zhai, M.G.; Hu, B.; Peng, P.; Zhao, T.P. Meso-Neoproterozoic magmatic events and multi-stage rifting in the NCC. Earth Science Frontiers. 2014, 21(1), 100-119 (in Chinese with English abstract).
45. Zhao, Z,P. Precambrian crustal evolution of the Sino-Korean Paraplatform. Beijing: Science Press (in Chinese). 1993.
46. Yang, C.S. Magmatism and mineralization in Huayangchuan ore concentration area in the western part of Xiaoqinling. Beijing: University of Chinese Academy of Sciences (in Chinese with English abstract). 2020.
47. Zhao, T.P.; Chen, F.K.; Zhai, M.G.; Xia, B. Single zircon U-Pb ages and their geological significance of the Damiao anorthosite complex, Hebei Province, China. Acta Petrologica Sinica. 2004, 20(3), 685-690 (in Chinese with English abstract).
48. Lu, S.N.; Zhao, G.C.; Wang, H.C.; Hao, G.J. Precambrian metamorphic basement and sedimentary cover of the North China Craton: A review. Precambrian Research. 2008,160(1-2), 77-93.
49. Peng, P., 2015. Precambrian mafic dyke swarms in the North China Craton and their geological implications. Science China (Earth Sciences) 58(5), 649-675.
50. Pearce, J.A.; Harris, N.B.W.; Tindle, A.G. Trace element discrimination diagrams for the tectonic interpretation of granitic rocks. Journal of Petrology. 1984, 25(4), 956-983. DOI:10.1093/petrology/25.4.956
51. Rogers, J.J.W.; Santosh, M. Tectonics and surface effects of the supercontinent Columbia. Gondwana Research. 2009, 15: 373-380.
52. Brown, G.C. Calc-alkaline intrusive rocks their diversity, evolution, and relation to volcanic arcs[C]//Thorpe R S(ed.). Andesites-orogenic Andesites and Related Rocks. New York: John Wiley & Sons. 1982, 437-464.
53. Batchelor, R.A.; Bowden, P. Petrogenetic interpretation of granitiod rock series using multi-cationic parameters. Chem. Geol. 1985, 48(1), 43-55.
54. Collins, W.J.; Beams, S.D.; White, A.J.R.; Chappell, B.W. Nature and origin of A-type granites with particular reference to southeastern Australia. Contributions to Mineralogy and Petrology. 1982, 80(2), 189-200.

 doi:10.20944/preprints202306.0870.v1

55. Creaser, R.A.; Price, R.C.; Wormald, R.J., 1991. A-type granites revisited: Assessment of a residual-source model. Geology 19(2): 163-166.
56. Yang, J.H.; Wu, F.Y.; Chung, S.L.; Wilde, S.A.; Chu, M.F. A hybrid origin for the Qianshan A-type granite, northeast China: Geochemical and Sr-Nd-Hf isotopic evidence. Lithos. 2006, 89 (1-2): 89-106.
57. Shellnutt, J.G.; Wang, C.Y.; Zhou, M.F.; Yang, Y.H. Zircon Lu-Hf isotopic compositions of metaluminous and peralkaline A-type granitic plutons of the Emeishan large igneous province (SW China): Constraints on the mantle source. Journal of Asian Earth Sciences. 2009, 35(1),45-55.
58. Zhao, X.F.; Zhou, M.F.; Li, J.W.; Wu, F.Y. Association of Neoproterozoic A- and I-type granites in South China: Implicationsfor generation of A-type granites in a subduction-related environment. Chemical Geology. 2008, 257(1-2):1-15.
59. Ni, Z.Y.; Wang, R.M.; Tong, Y.; Yang, C.; Dai, T.M. $^{207}Pb/^{206}Pb$ age of zircon and $^{40}Ar/^{39}Ar$ of amphibole from plagioelaseamphibolite in the Taihua group, Luoning, Henan, China. Geological Review. 2003, 49(4), 361-366 (in Chinese with English abstract).